Metformin alleviates insulin resistance in obese-induced mice via remodeling gut microbiota and intestinal metabolites

Ya Zhang [a,b,1], Yang Cheng [a,1], Jihui Zuo [a,1], Liping Yan [a], Qiaojuan Li [a], Ronald W. Thring [b], Yue Yang [a], Yitian Gao [a,*], Mingjiang Wu [a,*], Haibin Tong [a,*]

[a] College of Life and Environmental Science, Wenzhou University, Wenzhou 325035, China;

[b] Environmental Science and Environmental Engineering, University of Northern British Columbia, Prince George, BC, Canada;

*Correspondence: tonghaibin@gmail.com (H.T.); wmj@wzu.edu.cn (M.W.); gyt@wzu.edu.cn (Y.G.); Tel.: + 86-577-86689078

[1] These authors contributed equally to this study.

Abstract

Metformin is widely used to surmount insulin resistance (IR) and diabetes. Evidence indicates that metformin remodels gut microbiota but the underlying mechanism remain unclear. Present results showed that metformin effectively improved insulin sensitivity and alleviated liver inflammation and oxidative stress in high fat diet (HFD)-induced mice. Metabolomics analysis showed that metformin increased tauroursodeoxycholic acid (TUDCA) production by increasing the expression of bile acid synthase *Cyp7a1* and *Baat*. In the palmitic acid (PA)-induced cell, TUDCA activated Nrf2/ARE pathway, thereby reducing intracellular ROS and improving insulin signaling. Further gut microbiota analysis showed that metformin increased the proportion of *Akkermanisia muciniphlia* in the HFD-fed mice, while TUDCA promoted the proliferation of *A. muciniphlia* but metformin did not. These findings reveal that metformin remodels the gut microbiota, reduces oxidative stress and enhances insulin sensitivity by increasing the production of TUDCA. This provides a novel mechanism by which metformin alleviates diet-induced IR and improves metabolism.

Keywords: Metformin; Gut microbiota; Insulin resistance; Metabolomics; TUDCA; Nrf2

35 **Introduction**

36 The prevalence of obesity and overweight have been on the rise worldwide[1,2].
37 Current predictions indicate that more than 1 billion people will be obese by 2030[3].
38 Visceral obesity precedes the development of metabolic complications and chronic
39 diseases such as type 2 diabetes (T2D)[4], hepatic steatosis[5] and cardiovascular
40 diseases[6]. Metformin has been the first-line anti-diabetic drug for more than 60 years
41 because of its excellent hypoglycemic effect and safety profile[1,7]. Although several
42 studies have explored the mechanisms by which metformin maintains glucose
43 homeostasis, findings from such studies are inconsistent. The prevailing view is that
44 metformin activates AMP-activated protein kinase (AMPK) in the liver, similar to the
45 principle of caloric restriction that relieves symptoms of diabetes[8,9]. However,
46 metformin is an orally administered drug that reaches high concentrations in the
47 intestine with much lower serum concentrations[10], thus, the possibility that its
48 metabolic therapeutic mechanism might be due in part to actions in the intestine
49 cannot be ignored. Accumulated evidence shows that a high-fat diet (HFD) reduces
50 the abundance of *Lactobacilli* in the small intestine. However, this can be
51 counteracted by metformin, which increases the proportion of probiotics, thus,
52 relieving the symptoms of HFD-induced diabetes[11]. Although metformin may play a
53 hypoglycemic effect by improving the gut microbiota, oral administration of
54 antibiotics to diabetic mice impairs the hypoglycemic ability of metformin[12]. In
55 addition, while metformin can increase the abundance of *Escherichia coli*, it can as
56 well reduce the abundance of *Intestinibacter*. This can further influence diverse
57 biological processes such as the synthesis of branched-chain amino acid and the
58 secretion of GLP-1, thereby improving glucose tolerance and alleviating insulin
59 resistance (IR)[13,14]. These findings suggest that modulation of gut microbiota is
60 involved in the hypoglycemic mechanism of metformin.

61 Bile acids (BAs), which are produced in the liver and serve as important
62 ingredients of the digestive fluid in the intestine, enter the small intestine through the

63 biliary system and participate in fat digestion and absorption[15,16]. Gathered evidence
64 demonstrates that BAs could improve the intestinal homeostasis by modulating the
65 gut microbiota, thus relieving metabolic syndrome[17]. Recent studies also suggest that
66 BAs can participate in the liver-gut axis circulation and the improvement of
67 HFD-initiated metabolic disorders by inhibiting the proliferation of pathogenic
68 bacteria[18,19]. By modulating the gut microbiota, BAs have also been reported to
69 induce multiple beneficial effects on the intestinal lumen and intestinal walls such as
70 the suppression of intestinal inflammatory responses[20,21], the resolution of
71 endoplasmic reticulum (ER) stress in the intestinal epithelial cells underlying the
72 pathology of inflammatory bowel disease[22] and the improvement of gut barrier
73 dysfunction[23-25]. These findings suggest that there is a complex relationship between
74 BAs, gut microbiota and metabolic syndrome.

75 Previous studies have reported the association of BAs with oxidative stress,
76 which has been shown to treat metabolic dysfunction by acting as an endogenous
77 chemical chaperone to protect cells against ER stress[26]. Intestinal microenvironment
78 (including inflammation status, the function of the epithelial tight junction and gut
79 microbiota) plays an essential role in the progression of obese-induced IR. The
80 presence of gut microbiota and BAs in the intestine may be closely associated with
81 intestinal metabolic state. Analyses from metagenomic sequencing and metabolomics
82 show that metformin treatment increases the levels of the conjugated bile acid in the
83 gut by decreasing the abundance and bile salt hydrolase (BSH) activity of
84 *Bifidobacterium* species in the intestines of individuals with T2D[27-31]. BAs are signal
85 molecules that control the dynamic balance between energy metabolism and liver
86 protection. It has been reported that BAs change with obesity, IR[32] and nonalcoholic
87 steatohepatitis (NASH)[25]. However, the mechanism by which BAs alleviate
88 HFD-induced IR and the underlying role played by the gut microbiota during this
89 process are not clear.

90 This study investigated how metformin prevents the development of IR in
91 HFD-induced obese mice by modulating the dysbiosis of gut microbiota and
92 alteration metabolites. Exploring the mechanism behind this improves our knowledge
93 of gut microbiota and metabolic interactions underlying the anti-insulin resistance
94 effects of metformin.

95 **Methods**

96 **Chemicals and diet**

97 Metformin (purity ≥ 98%), choline (purity ≥ 98%) and taurine (purity ≥ 99%)
98 were obtained from Sigma-Aldrich (St. Louis, MO, USA). Tauroursodeoxycholic acid
99 (TUDCA, purity ≥ 99%) was purchased from Selleck (Houston, Texas, USA). Both
100 the normal chow diet (NCD, containing 10% fat by energy) and high-fat diet (HFD,
101 containing 60% fat by energy) were purchased from Beijing HFK Bio-Technology
102 Co., Ltd. (Beijing, China). Antibodies against Akt, phospho-Akt (Ser473), IRS-1,
103 phospho-IRS-1 (Ser307), AMPK, phospho-AMPK (Thr172), Keap1, IκB,
104 phospho-IκB (Ser32), p65, phospho-p65 (Ser536), GAPDH and β-tubulin were
105 obtained from Cell Signaling Technology (Beverly, MA, USA). Nrf2, phospho-Nrf2
106 (Ser40), and 4-HNE were purchased from Abcam (Cambridge, UK). Horseradish
107 peroxidase (HRP)–conjugated secondary antibody was obtained from Santa Cruz
108 Biotechnology (Santa Cruz, USA).

109 **Animal experiments**

110 Male ICR mice (7 weeks old, body weight 20 ± 1 g) were housed in ventilated
111 cages (four animals per cage) at the SPF facility of Wenzhou University under
112 controlled environmental conditions (temperature 22 ± 2°C; relative humidity
113 60–70%) with free access to standard laboratory chow and tap water. The mice were
114 maintained on a regular 12/12 h light/dark cycle. All animal care and experimental
115 procedures were approved by the Animal Care Ministry of Health and were
116 performed in accordance with the guide for the Care and Use of Experimental

117 Animals of Wenzhou University.

118 Mice were acclimatized to their environment for 1 week before the experiments.
119 Mice were randomly allocated into three groups (n = 9 for each group). A co-worker
120 blinded to the experimental protocol randomized animals into these groups. One
121 group of animals was fed with NCD and the other two groups were fed with HFD.
122 After 12 weeks of HFD feeding, one group of HFD-fed mice was administered
123 metformin (200 mg/kg body weight), once daily (HFD+Met group) for 6 weeks,
124 whereas the NCD-fed mice (NCD group) and other group of HFD-fed mice (HFD
125 group) were treated with an equal volume of saline for 6 weeks. The whole study
126 lasted 18 weeks, during which the body weight, water consumption and food intake
127 were measured every week. At week 18, intraperitoneal glucose tolerance test (IPGTT)
128 and intraperitoneal insulin tolerance test (IPITT) were performed as previously
129 described[33].

130 Fresh feces were collected and stored immediately at 80°C for subsequent
131 analysis. At the end of the trial, after overnight fasting for 12 h, blood samples were
132 collected, and serum was isolated by centrifugation at 1000 × *g* for 15 min at 4°C, and
133 stored at −80°C for further assay. Tissues, including the adipose tissue, liver and
134 ileum, were weighed; one portion of the tissues was fixed with 10% formaldehyde for
135 histological analysis, and the other portion was immediately frozen in liquid nitrogen
136 for further analysis.

137 Total cholesterol (T-CHO), triacylglycerol (TG), free fatty acids (FFA),
138 high-density lipoprotein (HDL-c), low-density lipoprotein (LDL-c), fasting blood
139 glucose (FBG), fasting serum insulin (FINS), catalase (CAT), malondialdehyde
140 (MDA), aspartate aminotransferase (AST), alanine aminotransferase (ALT), acid
141 phosphatase (ACP) and alkaline phosphatase (AKP), mice-lipopolysaccharides (LPS)
142 were determined by biochemical kits purchased from Jiancheng Bioengineering
143 Institute (Nanjing, China). The ratio of reduced glutathione (GSH) and oxidized

144 glutathione (GSSG) were determined by a GSH:GSSG kit (Jiancheng Bioengineering
145 Institute, Nanjing, China). Homeostasis model assessment-estimated insulin
146 resistance (HOMA-IR) was calculated using the following formula:

147 HOMA-IR = FBG (mmol/L) × FINS (mU)/22.5

148 **Hematoxylin and eosin staining**

149 Samples were fixed in 10% formaldehyde overnight, paraffin-embedded,
150 sectioned (4-μm thickness, 3–5 sections/specimen) and stained with hematoxylin and
151 eosin (H & E) for histological analysis. Digital images of H & E stained sections were
152 acquired with a Nikon Eclipse Ti microscope at ×400 magnifications (Ti-E/U/S,
153 Japan). Image J software (National Institutes of Health, USA) was used to count
154 adipocytes.

155 **Cell culture**

156 Human liver hepatocellular carcinoma (HepG2) cells were cultured in MEM
157 (Sigma, St. Louis, MO, USA) supplemented with 10% FBS (Gibco, South American),
158 penicillin and streptomycin. Cells were maintained in 5% CO_2 at 37°C.

159 **siRNA Transfection**

160 *Nrf2* was knocked-down by RNA interference (RNAi) using the following 19-bp
161 (including a 2-deoxynucleotide overhang) siRNAs (Origene, Beijing, China): *Nrf2*,
162 SR321100A-AUUGAUGUUUCUGAUCUAUCACUTT;
163 SR321100B-GUCAGUAUGUUGAAUCAGUAGUUTC;
164 SR321100C-CCAGUCUUCAUUGCUACUAAUCAGG. Stealth RNAi (Origene,
165 Beijing, China) was used as a negative control (siCont). For transfection, cells were
166 seeded on a six-well plate, grown to ~80% confluence and transfected with siRNA
167 duplexes using Lipofectamine 3000 (Invitrogen, Camarillo, CA, USA) according to
168 the manufacturer's recommendations. After incubation for 48 h, the expression level
169 of Nrf2 protein was detected by western blot.

170 **Glucose uptake assay**

171 Cells were plated at 1 x 10^4/well in 96-well plates and used at subconfluence
172 after 24 h of preincubation. For experiments, all culture medium was removed from
173 each well and replaced with 100 μM fluorescent
174 2-Deoxy-2-[(7-nitro-2,1,3-benzoxadiazol-4-yl) amino]-D-glucose (2-NBDG)[34] in
175 serum-free medium and incubated for 30 min. Subsequently, cells were washed thrice
176 with PBS and then the fluorescence intensity was determined with a fluorescence
177 microplate reader (Ex/Em, 488/520 nm). The glucose concentration in the medium
178 supernatant was determined by a glucose detection kit (Jiancheng Bioengineering
179 Institute, Nanjing, China) following the manufacturer's instructions.

180 **Flow cytometry assays**

181 The reactive oxygen species (ROS) level was evaluated by flow cytometry
182 (FACSCanto II, BD, USA) using the DCFDA cellular reactive oxygen species
183 detection assay kit (Byotime, Shanghai, China) according to the manufacturer's
184 protocol. Cells were briefly stained with 2′,7′-dichlorofluorescein diacetate (DCFA) at
185 37°C for 30 min, washed with 1× PBS buffer, and the signal was read at an excitation
186 of 485 nm and an emission of 535 nm.

187 **Quantitative RT-PCR**

188 Total mRNA was isolated from tissue samples using TRIzol reagent (TAKARA,
189 Tokyo, Japan) and was reverse-transcribed into cDNA using a high-capacity cDNA
190 reverse transcription kit (TAKARA, Tokyo, Japan) according to the manufacturer's
191 protocol. The mRNA levels were quantified with quantitative PCR (qPCR) using
192 SYBR Green (Qiagen, Hilden, Germany). Amplification was performed on a
193 LightCycler480 *q*RT-PCR system (Roche, Mannheim, Germany) under the following
194 reactions: 95°C for 15 min, followed by 40 cycles at 95°C for 10 s, 60°C for 20 s, and
195 72°C for 20 s. The relative mRNA levels of target genes were normalized to the
196 expression of GAPDH calculated using $2^{-\Delta\Delta ct}$ method. The primer pairs used in this

197 study are listed in Supporting table.

198 **Western blot analysis**

199 Samples were homogenized with ice-cold RIPA lysis buffer containing protease
200 and phosphatase inhibitors (Beyotime, Shanghai, China). The homogenates were
201 centrifuged at 10 000 × *g* for 20 min at 4°C to remove the insoluble tissue debris. The
202 protein concentration in the supernatant was determined using a BCA protein assay
203 kit (Beyotime, Shanghai, China) according to the manufacturer's protocol. Equal
204 amount of protein for each group were denatured in boiling water for 5 min. Aliquots
205 (40 μg) of protein samples were subjected to 10% SDS-PAGE and transferred to
206 PVDF membranes (Millipore, Bedford, MA, USA). After blocking with 5% nonfat
207 milk (dissolved in TBST) for 1 h, the membranes were incubated with the indicated
208 antibodies at 4°C overnight, followed by incubation with the appropriate
209 HRP-conjugated second antibodies for 1 h at room temperature. Chemiluminescent
210 detection was performed using the ECL Plus Western blotting reagent (TransStart,
211 Beijing, China). Semi-quantitative analysis for densitometry of each band was
212 performed using ImageJ software.

213 **Analysis of gut microbiota by 16S rRNA amplicon sequencing**

214 As described previously[11], total bacterial DNA was extracted from the collected
215 feces using CTAB/SDS method. Illumina MiSeq (Novogene Bioinformatics
216 Technology Co., Ltd.) was used to analyze the 16S rRNA genes in the DNA sample
217 to determine the composition and diversity of bacteria. Sample processing, data
218 acquisition and analysis were described in full detail in Supplementary
219 methodologies.

220 **Non-targeted metabolome analysis**

221 A non-targeted metabolome analysis of the colon contents was performed with a
222 liquid chromatography-tandem mass spectrometry (LC-MS) method (Waters

223 ACQUITY UPLC (Waters, America) coupled to a Thermo LTQ Orbitrap XL system
224 (Thermo, America)). Sample processing, data acquisition, UPLC conditions and data
225 analysis were described in full detail in the Supplementary methodologies.

226 **Growth curve of *Akkermansia muciniphila***

227 ***Akkermansia*** *muciniphila* strain ATCC BAA-835 was purchased from the
228 Beinan (Beijing, China). Bacteria were cultured in BHI medium in tubes at 37°C in an
229 anaerobic chamber (Whitley A35 Workstation 2.5, Don Whitley Scientific, UK). To
230 acquire the growth curve of *A. muciniphila*, the medium in test tubes supplemented
231 with or without 10 mM metformin (or 200 μM TUDCA) was placed in an anaerobic
232 bag to eliminate oxygen for 24 h. The test tubes were then inoculated with bacteria
233 and incubated at 37°C in an anaerobic bag. The OD_{600} of the cultures was measured
234 every 3 hours.

235 **Determination of hepatic TUDCA**

236 The contents of TUDCA in hepatic tissues were determined by
237 high-performance liquid chromatography (HPLC). Briefly, 200 mg of frozen tissue
238 was homogenized with a TissueLyserII (Qiagen, Germantown, MD, USA) in 1 mL of
239 PBS to prepare the tissue homogenates. The impurities were removed through a 0.22
240 μm filter, then the filtrate was precipitated by methanol and 10 μL of supernatant was
241 analyzed using an Agilent 1290 HPLC system (Santa Clara, CA) equipped with a
242 Hypersil ODS-2 column (5 μm, 4.6 × 250 mm; Waters, USA). The supernatant was
243 detected at the wavelength of 210 nm, eluted with the mobile phase of 0.03 M
244 phosphate buffer solution (pH 4.4) and methanol (32:68, v/v) at a flow rate of 1.0
245 mL/min.

246 **Statistical analysis**

247 Statistical comparisons among experimental groups were analyzed by one-way
248 ANOVA and Duncan's multiple-comparison test using the SPSS software (Version

249 21.0. Armonk, NY: IBM Corp.). *P* values less than 0.05 were considered statistically
250 significant.

251 **Results**

252 **1. Metformin prevents diet-induced obesity and increases insulin sensitivity**

253 To assess the efficacy of metformin on the treatment of obese mice with IR,
254 animals were divided into the NCD, HFD and HFD + Met groups. Daily oral
255 administration of metformin significantly alleviated diet-induced body weight
256 increase from day 14 onwards (**Figure 1A)**. At the end of metformin treatment, the
257 weight gain and BMI were also significantly decreased (**Figure 1B, Supplementary**
258 **Figure 1a)**, without affecting food intake (**Figure 1C**). Metformin prevented fat
259 deposition in the subcutaneous adipose, the adipose index (**Supplementary Figure**
260 **1b)** and H & E staining of adipose tissue (**Figure 1D).** Adiposity numbers showed
261 that metformin effectively ameliorated adipocyte hypertrophy (**Figure 1E**). The
262 indexes of the pancreas and kidney were not affected by metformin administration.
263 The liver index was significantly reduced in metformin-treated mice (**Supplementary**
264 **Figure 1b**). The diet-induced hepatic steatosis and dyslipidemia were effectively
265 prevented by metformin treatment as indicated by the lower concentration of T-CHO,
266 TG and FFA in both the liver and the serum of the HFD + Met group compared with
267 the HFD group (**Figure 1 F-H**). We also found that metformin could effectively
268 prevent hepatocyte damage. This was evidenced by the lower levels of AST, ALT,
269 ACP and AKP in the serum (**Supplementary Figure 2**).

270 Glycemic homeostasis was determined by IPGTT and IPITT. As shown in
271 **Figure 2A**, the oral administration of glucose increased the blood glucose (BG) level
272 within 30 min in the HFD-fed mice, which remained high for the subsequent 90 min.
273 This indicated that HFD feeding markedly impaired glucose tolerance. In addition, the
274 BG of the NCD group peaked within 30 min but dropped to the normal level after 120
275 min. Metformin significantly inhibited the rise of BG level and enhanced glucose

276 clearance in the HFD-fed mice after oral administration of glucose. The results of
277 IPGTT were expressed as the area under the curve (AUC) of BG over 120 min. The
278 AUC of the HFD + Met group was significantly decreased compared with that of the
279 HFD group (**Figure 2B**, $P < 0.05$). The improvement of insulin resistance (IR) was
280 also supported by the results of IPITT. After intraperitoneally injected insulin at 0.75
281 U/kg, the BG levels at 30, 60, and 120 min revealed that the mice in the HFD + Met
282 group took more advantage of insulin compared with the mice in the HFD group
283 (**Figure 2C**). The significant difference ($P < 0.05$) of the slope between the HFD
284 group and the HFD + Met group suggested that metformin increased the utilization of
285 insulin and improved insulin sensitivity in the HFD-fed mice (**Figure 2D**). Moreover,
286 the FBG level in the HFD group was significantly higher compared to that in the
287 NCD group. Compared with the HFD group, the mice treated with metformin had a
288 lower FBG level (**Figures 2E**). Marked elevation in fasting serum lisulin (FINS) was
289 observed in the HFD group compared with the NCD group. Notably, metformin
290 treatment tended to reverse the increase in FINS (**Figure 2F**). HOMA-IR is an
291 indicator for evaluating the level of insulin resistance in an individual. Based on the
292 HOMA-IR analysis, we found that the HOMA-IR of the HFD + Met group was
293 comparable to that of the NCD group but significantly lower compared with that of
294 the HFD group (**Figure 2G**).

295 PI3K/Akt and insulin receptor substrate-1 (IRS-1) are the main signaling
296 molecules in the signaling pathway of the insulin receptor. The level of
297 phosphorylated Akt at Ser473 was significantly reduced in the liver of the
298 HFD-induced obese mice, but the level was restored in the HFD + Met group (**Figure**
299 **2H**). Contrary to the phosphorylated Akt, the level of phosphorylated IRS-1 at Ser307
300 was significantly elevated in the HFD group, whereas in the HFD + Met group, the
301 level was reduced. These results indicate that the preventive effect of metformin on
302 HFD-induced obesity resulted in improved glucose homeostasis and insulin
303 sensitivity.

304 **2. Metformin alleviates HFD-induced inflammation and oxidative stress**

305 As shown in **Figure 3A** and **3B**, metformin prevented metabolic inflammation in
306 the liver and ileum, leading to an increased tendency towards reduced gene expression
307 of interleukin-1β (*Il-1β*), interleukin-6 (*Il-6*) and tumor necrosis factor-α (*Tnf-α*) in the
308 ileum. However, there was no effect on interleukin-10 (*Il-10*). Metformin also
309 prevented the release of endotoxin, which was indicated by lower levels of LPS in
310 serum (**Figure 3C**). Meanwhile, the phosphorylated levels of p65 and IκB were
311 decreased in the livers of metformin-treated mice compared with the HFD-fed mice
312 (**Figure 3D**). This indicated that the HFD-induced activation of NF-κB signaling was
313 suppressed by metformin.

314 To investigate the involvement of oxidative stress in the development of HFD-
315 induced IR, we first measured the activity of the antioxidant enzyme in both the
316 plasma and the liver. The results showed that the activities of CAT in the serum and
317 the liver were markedly lower in the HFD group compared with the NCD group
318 (**Figure 4A**). In addition, the ratio of GSH/GSSG was reduced (**Figure 4C**). After
319 metformin intervention, the activities of CAT and the ratio of GSH/GSSG were
320 significantly increased. The accumulation of lipid peroxide, caused by HFD, was
321 improved in the metformin group (**Figure 4B**). This was exhibited by the significantly
322 reduced MDA level in the liver. Nrf2/ARE is a classic antioxidant-signaling pathway
323 and KEAP1 is a key protein that mediates the degradation of Nrf2. HFD feeding
324 significantly inhibited Nrf2/ARE signaling (**Figure 4D**) whereas metformin
325 significantly increased the expression of Nrf2. Nrf2/ARE signaling regulates the
326 expression of a variety of detoxification and antioxidant enzymes. As shown in
327 **Figure 4E**, Metformin significantly up-regulated the mRNA levels of *Nqo1* and *Ho1*,
328 which are essential genes for balancing oxidative stress. These results indicate that
329 metformin can improve intestinal and hepatic inflammation, oxidative stress and lipid
330 peroxide accumulation in HFD-fed mice.

331 **3. Metformin prevents obesity-driven dysbiosis of gut microbiota and reshapes**
332 **intestinal metabolites**

333 Faecal samples were collected for gut microbiota analysis by 16S rRNA
334 amplicon sequencing. Following all quality trimming and checking, a dataset
335 consisting of 80004, highly qualified reads, was collected for subsequent analysis.
336 Our data showed that the numbers of unique OTUs in the NCD, HFD, and HFD +
337 Met groups were 372, 350 and 374, respectively. The coverage of sequencing results
338 was nearly complete for all sequences in the three groups, demonstrating sufficient
339 sequencing depth for follow-up analyses. The metformin-treated group significantly
340 increased the Ace and Chao1 indices compared with the HFD group (**Table 1**).
341 Metformin-treated mice, however, clustered partially apart from HFD-fed mice
342 samples, suggesting important changes in metformin gut microbial profile (**Figure**
343 **5A**). Metformin treatment prevented HFD-induced decrease in Bacteroidetes and the
344 increase in the Firmicutes/Bacteroidetes ratio (**Figure 5B** and **C**), two hallmarks of
345 obesity-driven dysbiosis. Based on FunGuild and FAPROTAX analysis of flora
346 function, the HFD group showed a decrease in the proportion of the
347 chemoheterotrophy and the fermentation bacteria when compared with the NCD
348 group (**Figure 5D**). However, after metformin supplementation reshaped the structure
349 of gut microbiota, chemoheterotrophy and fermentation improved in the HFD + Met
350 group. Heatmap presents the clustering of bacterial communities with their relative
351 abundances at the genus level (**Figure 6A)**. Compared with the NCD group, unique
352 high-abundance bacteria in the HFD group are mainly concentrated in
353 *Bifidobacterium, Roseburia, Lachnoclostridum, Alloprevotella* and *Mucispirilum*.
354 However, metformin decreased the abundance of these bacteria, making the
355 metformin-treated group comparable to the NCD group. In addition, metformin
356 specifically increased the abundance of *Butyricimonas, Parasulterella,*
357 *Parabacteroides* and *Akkermansia*. Consistent with the decrease in F/B ratio as shown
358 in **Figure 5C**, the difference between the HFD group and the HFD + Met group is

359 mainly reflected in the decrease in the abundance of Firmicutes and the increase in the
360 abundance of Bacteroidetes (**Figure 6B**). Compared with the NCD and HFD + Met
361 groups, *c_Erysipelotrichia, f_proteobacteria, g_Turicibacter, o_Bifidobacteriales* and
362 *s_Clostridium* in the HFD group were significantly up-regulated, whereas
363 f*_Muribaculaceae, g_parabacteroides* and *f_tannerellaceae* were significantly
364 up-regulated in the HFD + Met group. Therefore, metformin can increase the
365 abundance of Bacteriodia at the phylum level and *Parabacteroides* at the genus level,
366 and modulate HFD-induced dysbiosis of gut microbiota.

367 The intestinal metabolite profiles were further measured using lipid
368 chromatography and mass spectrometry (LC-MS) to reveal the influences of
369 metformin on the intestinal metabolites. When comparing the HFD group and HFD +
370 Met group, metabolites were dictated by metformin. For instance, in the HFD group,
371 118 up-regulated metabolites were identified, whereas 182 down-regulated
372 metabolites were established in the HFD + Met group (**Figure 7A-C**). The HFD +
373 Met group effectively increases the content of taurine, choline and TUDCA in the
374 intestine compared with the HFD group (**Figure 7D**). This is consistent with previous
375 reports[18]. Collectively, these results showed that metformin administration altered the
376 intestinal metabolites and the gut microbiota. **Figures 8A** and **8B** showed the
377 correlation between intestinal metabolism and the gut microbiome at the phylum and
378 species level after the intervention of metformin in HFD-fed mice. TUDCA was
379 highly associated with *A. muciniphila* species belonging to the *Verrucomicrobia*
380 phylum. Interestingly, through the analysis of growth curves, it was not metformin but
381 TUDCA significantly accelerated the proliferation of *A. muciniphila in vitro* (**Figure**
382 **8**C). These data suggest that metformin may indirectly improve insulin resistance
383 caused by a high-fat diet through modulation of the structure of gut microbiota and
384 metabolites.

385 **4. TUDCA improves PA-induced insulin resistance and lipid peroxidation**

386 Further study was carried out to determine whether TUDCA could alleviate
387 hepatic insulin resistance using a PA-treated HepG2 cell model. PA exposure (200
388 μM) resulted in a decrease in glucose uptake in HepG2 cells. This was demonstrated
389 by the reduction of fluorescence density in the cytoplasm (**Figure 9A**) and the high
390 concentration of glucose in the medium (**Figure 9B**). In addition, PA decreased the
391 level of phosphorylated Akt at Ser473 and increased phosphorylated IRS-1 level at
392 Ser307, thus, revealing a typical symptoms of insulin resistance (**Supplementary**
393 **Figure 3**). As shown in **Figure 9A** and **9B**, the impaired glucose uptake caused by PA
394 was significantly alleviated by TUDCA, excluding choline and taurine
395 (**Supplementary Figure 4**). Moreover, the suppressed phosphorylation level of Akt
396 in PA-treated HepG2 cells was elevated by TUDCA, while the phosphorylated IRS-1
397 level at Ser307 was also significantly reduced (**Figure 9C**). Note that, TUDCA
398 treatment at high doses may produce toxic side effects and fail to exert insulin
399 sensitization. These findings confirmed that TUDCA could improve hepatic glucose
400 intolerance and enhance insulin sensitivity of PA-treated hepatocyte in a
401 metformin-independent manner.

402 Homeostasis imbalances on glucose metabolism often cause inflammation and
403 oxidative stress damage in hepatic cells. Thus, we further investigated whether
404 TUDCA could alleviate these pathological processes. The intracellular ROS content
405 was visualized by using the DCF-DA dye and flow cytometric platform. **Figure 10A**
406 showed that PA could increase ROS generation in the HepG2 cells. Interestingly,
407 TUDCA significantly decreased PA-induced ROS generation. On the other hand, the
408 ratio of GSH/GSSG was significantly increased by TUDCA (**Figure 10B**). In addition,
409 pro-inflammatory cytokines such as *Tnf-α*, *Il-1β* and *Il-6* were also significantly
410 reduced by TUDCA treatment at mRNA level (**Supplementary Figure 5**).

411 We further investigated whether TUDCA alleviates PA-induced insulin
412 resistance through the Nrf2/ARE signaling pathway. The transcriptional activity of
413 Nrf2 was determined by measuring the mRNA levels of its representative downstream

414 target genes. TUDCA significantly up-regulated the expression of Nrf2, suppressed
415 by PA (**Figure 10D**). It also up-regulated the expression of antioxidant genes, *Ho-1*,
416 *Nqo1*, *Cat* and *Gpx4*, downstream of the Nrf2/ARE signaling pathway (**Figure 10D**).
417 We found that TUDCA was unable to alleviate PA-induced insulin resistance in
418 HepG2 cells that interfered with Nrf2 expression (**Supplementary Figure 6**, **10E &**
419 **F**). Together, the results suggest that TUDCA may significantly activate the
420 Nrf2/ARE signaling, thereby enhancing antioxidant capacity, and alleviating insulin
421 resistance in the HepG2 cells caused by PA.

422 To further determine the source of TUDCA, we detected the TUDCA content in
423 the liver of the HFD and the HFD + Met groups. As shown in **Figure 11A**, TUDCA
424 in the liver of the HFD + Met group (5.281 ± 0.745 nmol/g) was significantly
425 increased compared with that in the HFD group (2.992 ± 0.691 nmol/g). In the HFD +
426 Met group, the gene expression of *Cyp7a1* and *Baat*, the important enzymes involved
427 in the biosynthesis of TUDCA, was significantly up-regulated compared with that in
428 the HFD group (**Figure 11B**). This suggests that metformin can promote the
429 production of TUDCA in the liver by up-regulating the enzymes that limit the rate of
430 TUDCA biosynthesis, and *Cyp7a1* and *Baat* expression.

431 **Discussion**

432 Metabolic syndromes such as obesity, nonalcoholic fatty liver disease and T2D
433 are increasingly prevalent globally, especially in recent decades[2]. Metformin, the most
434 widely used anti-diabetic drug worldwide, has been reported to favorably influence
435 metabolic and cellular processes. Metformin is also shown to be closely associated
436 with the development of insulin resistance[35,36]; however, the mechanism is still not
437 clear. Recent studies have revealed that the development of metabolic disease
438 strongly correlates to the accumulation of gut microbiota and metabolites. Multiple
439 studies have investigated the impact of metformin on the gut microbiota, metabolism
440 and related host targets on the regulation of glucose metabolism[37,38]. We explored the

441 potential mechanism involving the gut microbiota and intestinal metabolites to reveal
442 how metformin improves diet-induced obesity and insulin resistance. We established
443 that the daily administration of metformin strongly ameliorated the obesity-related
444 interruption of gut microbiota. The bile acid TUDCA was maintained at a high level
445 in the intestine, which in turn promoted the proliferation of *A. muciniphila*, improved
446 the integrity of the intestinal wall and reduced intestinal inflammation. Furthermore,
447 TUDCA was identified as an activator of Nrf2/ARE signaling in hepatocyte that
448 decreased oxidative stress imbalance, while improving hepatic inflammation and
449 insulin resistance in HFD-induced obese mice.

450 T2D is both an inflammatory and a natural immune disease. There is a variety of
451 microbiota in the human intestine, which is involved in body immunity, infection and
452 nutrient metabolism, and they are closely associated with the occurrence of diabetes.
453 The gut microbiota imbalance in composition and diversity can result in the release of
454 bacterial endotoxin. This could lead to chronic inflammation and destruction of the
455 normal physiological functions of tissues and organs. Several studies have confirmed
456 that chronic inflammation can cause insulin resistance and subsequently diabetes. The
457 decrease in Firmicutes/Bacteroidetes ratio is considered to be an indicator of
458 improved metabolism by metformin therapy[39,40]. LDA analysis showed that the
459 decreased abundance of Firmicutes by metformin could be due to the decrease in
460 *Erysipelotrichia* species, which belongs to the Firmicutes phylum. The role of
461 *Erysipelotrichia* species in human disease may be well established in studies
462 investigating metabolic disorders[41]. For instance, a previous study showed a bloom of
463 species belonging to the *Erysipelotrichaceae* family (initially classified as *Mollicutes*)
464 in diet-induced obese animals[42]. Within the host, *Erysipelotrichia* species appear to be
465 highly immunogenic[43], however, in surplus, they induce intestinal inflammation.
466 Studies have shown that species in *Erysipelotrichaceae* are positively correlated with
467 TNFα and IL-6 in the intestine and the liver[44].

468 In contrast, most of the bacteria up-regulated by metformin were probiotics. For
469 example, species in *Muribacaceae* are involved in the L-citrulline nitrogen metabolic
470 cycle. They scavenge free radicals, improve immunity and maintain blood glucose.
471 Metformin also up-regulates the abundance of *Parabacteroides*, including *P.*
472 *distasonis* and *P. goldsteinii*. Liu et al.[45] found that *P. distasonis* could transform bile
473 acids, activate intestinal gluconeogenesis through succinic acid and improve the host
474 metabolic disorders. In another study, Wu et al.[46] recorded that *P. goldsteinii* reduces
475 systemic inflammation and increases insulin sensitivity by maintaining intestinal
476 integrity. *Akkermansia muciniphila* is known to effectively alleviate intestinal
477 inflammation caused by obesity. Patients with intestinal obesity have been shown to
478 have a significantly reduced abundance of *A. muciniphila* compared with healthy
479 individuals. Numerous studies have demonstrated that metformin could up-regulate
480 the abundance of *A. muciniphila* in HFD-fed mice intestine, maintain the integrity of
481 the intestinal wall as well as effectively improve intestinal inflammation[47]. The
482 abundance of *A. muciniphila* is also significantly upregulated in the HFD + Met group.
483 As a mucin-degrading bacterium, the use of *A. muciniphila* has been shown to reduce
484 inflammation, maintain the intestinal barrier and increase levels of endocannabinoids
485 secreted by intestinal peptides[48]. We speculate that the transformation of gut
486 microbiota by metformin is the defining factor in improving chronic inflammation in
487 the intestine and even the whole body. Metformin can effectively inhibit the number
488 of pathogenic bacteria and promote the proliferation of probiotics. A suppression of
489 pathogenic bacteria coupled with a proliferation of probiotics may synergistically
490 reduce intestinal inflammation and maintain the integrity and permeability of the
491 intestinal wall. Furthermore, this may lead to a decrease in serum LPS and
492 improvement of systemic inflammation caused by HFD-induced obesity.

493 The "dialogue" between the gut microbiota and the organism mainly depends on
494 microbial metabolites. By producing various enzymes for biochemical metabolic
495 pathways of the intestinal microbes, gut microbiota can perform diverse metabolic

496 activities such as the metabolism of amino acids, carbohydrates and bile acids, as well
497 as the formation of a co-metabolic relationship with the host. Bile acids produced by
498 the gut microbiota are essential in the regulation of glycolipids and energy. Studies
499 have shown that in human primary hepatocytes, bile acids promote the β-oxidation of
500 fatty acids by activating FXR[18,49] and up-regulate the expression of apolipoprotein CII
501 gene to reduce the triglyceride content in the liver[21].

502 As a conjugated bile acid derivative, TUDCA has been shown to treat
503 nonalcoholic fatty liver disease (NAFLD) by acting as an endogenous chemical
504 chaperone; to protect cells against ER stress[26,50,51] and to reduce liver steatosis[52].
505 Moreover, TUDCA can alleviate dextran sulfate sodium-induced colitis in mice[53,54].
506 *In vitro*, we found that TUDCA could act as an agonist of the Nrf2/ARE signaling
507 pathway. This is reminiscent of the expression pattern of Nrf2, a crucial stress
508 regulator to reduce the ROS, which is a key factor in sensitizing insulin signaling[55-57].
509 It has also been confirmed that up-regulation of the Nrf2 expression both by genetic
510 manipulation and pharmacological interference, can significantly decrease the content
511 of ROS and ameliorate IR and T2D[58,59]. In the mice supplement with metformin, the
512 significant up-regulation in the expression of *Nrf2* and its downstream target genes
513 (*Gclc*, *Cat* and *Ho-1*) occurred, which further alleviated IR and over-oxidation.
514 Conversely, the stress-resistant effect of TUDCA was dramatically repressed by the
515 inhibition of the Nrf2/ARE signaling. *In vitro* experiments have found that TUDCA
516 have similar effects, which can effectively reduce the inflammation and oxidative
517 stress caused by PA as well as decreasing the accumulation of lipid peroxide. This
518 might be a novel mechanism for metformin in the treatment of insulin resistance and
519 diabetes.

520 In our present study, metabolomics data showed that TUDCA in the intestinal
521 contents of the HFD + Met group increased significantly. Previous studies revealed
522 that metformin treatment increased the levels of the conjugated bile acid in the gut by
523 decreasing the abundance of species of *Bifidobacterium* and its bile salt hydrolase

524 (BSH) activity in the intestines of individuals with T2D[17,30,31]. Bile salt hydrolase,
525 secreted by intestinal bacteria, decomposes TUDCA in the intestine and metabolizes
526 TUDCA to taurine and UDCA. However, data from the gut microbiota showed that
527 metformin did not affect the abundance of *Bifidobacterium* and *Lactobacillus*, the
528 major BSH-producing bacteria. In addition, we found that the content of taurine in the
529 intestine increased significantly. *In vitro*, TCDCA can be transformed into TUDCA
530 by 7α/β-hydroxysteroid dehydrogenase (7α/β-HSDH)[15,35,60]. Data from the gut
531 microbiota also revealed that metformin did not affect the abundance of *Eubacterium*
532 and *Clostridium*, the major 7α/β-HSDH-producing bacteria. Therefore, the increase in
533 TUDCA in the intestine is purportedly not due to the inhibitory effect of metformin
534 on BSH-producing bacteria. Further analysis of the biosynthetic site of bile acids and
535 the liver confirmed that the conjugated bile acid TUDCA was generated in the liver
536 through a series of catalytic reactions and enzymes such as CYP7A1 and BAAT.
537 CYP7A1 is a rate-limiting enzyme that catalyzes the breakdown of cholesterol into
538 bile acids in the liver[15,61] whereas BAAT is a vital enzyme that catalyzes the
539 amidation reaction of taurine and UDCA[46,62]. Interestingly, we found that the gene
540 expressions of *Cyp7a1* and *Baat* were significantly enhanced in the HFD + Met group,
541 which might further promote the synthesis of TUDCA in the liver. HPLC analysis
542 also showed an increase in the content of TUDCA in the livers of the HFD + Met
543 group. We suppose that the increase in TUDCA biosynthesis may be the primary
544 cause of the increase in TUDCA in the intestine.

545 Overall, in our present study, metformin was found to increase the bile acid
546 TUDCA production by increasing bile acid synthase *Cyp7a1* and *Baat.* As an
547 activator of the Nrf2/ARE signaling pathway, TUDCA promotes Nrf2
548 phosphorylation at Ser40. It also increases the gene transcription of its downstream
549 antioxidant enzyme, reduces oxidative stress and sensitizes insulin signaling; thereby
550 alleviating insulin resistance caused by HFD. The increase of TUDCA levels in the
551 intestine corresponded to the increase in the abundance of *A. muciniphlia.* Metformin

552 remodels the gut microbiota by promoting probiotics such as *Muribacaceae,* and
553 *Parabacteroides*, and inhibiting pathogenic bacteria such as *Erysipelotrichia* and
554 *Helicobacter*. This maintains intestinal integrity and reduces inflammation induced by
555 HFD. However, for a better understanding of the crucial mechanisms involved in the
556 long-term treatment with metformin in humans, the role of the intestine-liver axis
557 should be explored. Since *A. muciniphlia* and/or TUDCA are the novel target of
558 metformin in the gut, they are potential targets for the treatment of metabolic
559 conditions in humans.

560

561 **Conflict of Interest**

562 The authors declare no conflict of interest.

563

564 **Author Contributions**

565 Y.Z., Y.C., L.Y and J.Z. performed the research. H.T., Y.G. and M.W. designed
566 research. Y.Z., Q.L. and S.W. provided technical assistance. H.T. and Y.Z. analyzed
567 the data. Y.Z. and H.T. wrote the paper. H.T., Y.G. and M.W. had primary
568 responsibility for final content. All authors have read and approved the final
569 manuscript.

570

571 **Acknowledgements**

572 We thank Chujun Lin, Yufeng Wu, Lingfeng Hou, Huijing Jiang (Wenzhou
573 University) for their assistance in animal experiments. We thank Alan K Chang
574 (Wenzhou University) for helpful discussion and for revising the language of the
575 manuscript.

576

Funding

This work was financially supported by the National Natural Science Foundation of China (41876197 and 81872952), the National Key Research and Development Project (2018YFD0901503), the Natural Science Foundation of Zhejiang Province (LY18C020006), the Science and Technology Program of Wenzhou (ZY2019013 and Y20180210).

584 **References**

585 1. Muoio DM, Newgard CB. Mechanisms of disease:Molecular and metabolic
586 mechanisms of insulin resistance and beta-cell failure in type 2 diabetes. *Nat.*
587 *Rev.Mol. Cell Bio.* 2008; 9, 193-205. doi: 10.1038/nrm2327
588 2. Igel LI, Saunders KH, Fins JJ. Why weight? An analytic review of obesity
589 management, diabetes prevention, and cardiovascular risk reduction. *Cur. Athero.*
590 *Repor*. 2018; 20: 39. doi: 10.1007/s11883-018-0740-z
591 3. Abarca-Gómez L, Abdeen ZA, Hamid ZA, Dika Z, Ivkovic V, Jelakovic A,
592 Jelakovic B, Kos J, Jureša V, Majer M, et al. Worldwide trends in body-mass
593 index, underweight, overweight, and obesity from 1975 to 2016: a pooled
594 analysis of 2416 population-based measurement studies in 128·9 million children,
595 adolescents, and adults. *Lancet.* 2017; 390: 2627-2632. doi:
596 10.1016/s0140-6736(17)32129-3
597 4. Shen J, Obin MS, Zhao L. The gut microbiota, obesity and insulin resistance.
598 *Mol. Aspec. of Medic.* 2013; 34(1):39-58. doi: 10.1016/j.mam.2012.11.001
599 5. Bäckhed F, Manchester JK, Semenkovich CF, Gordon JI. Mechanisms
600 underlying the resistance to diet-induced obesity in germ-free mice. *P Natl. Acda.*
601 *Sci. USA*. 2007;104(3):979-984. doi: 10.1073/pnas.0605374104
602 6. Cho NH, Shaw JE, Karuranga S, Huang Y, Rocha Fernandes JD, Ohlrogge
603 AW, Malanda B. IDF diabetes atlas: global estimates of diabetes prevalence for
604 2017 and projections for 2045. *Diabetes. Res. Clin. Pract.* 2018; 138: 271-281.
605 doi: 10.1016/j.diabres.2018.02.023
606 7. Graham R. Hardie DG. Pearson RE. The mechanisms of action of metformin.
607 *Diabetologia*. 2017; 60:1577-1585. doi: 10.1007/s00125-017-4342-z
608 8. Zhou G, Myers R, Li Y, Chen Y, Shen X, Fenyk-Melody J, Wu M, Ventre J,
609 Doebber T, Fujii N, Musi N, Hirshman MF, Goodyear LJ, Moller DE. Role of
610 AMP-activated protein kinase in mechanism of metformin action. *J Clin Invest.*
611 2001; 108:1167-74. doi: 10.1172/JCI13505

612 9. Hawley SA, Ross FA, Chevtzoff C, Green KA, Evans A, Fogarty S,
613 Towler MC, Brown LJ, Ogunbayo OA, Evans AM, Hardie DG. Use of cells ex-
614 pressing gamma subunit variants to identify diverse mechanisms of AMPK
615 activation. *Cell Metab.* 2010; 11:554-565. doi: 10.1016/j.cmet.2010.04.001
616 10. Lee H, Ko G. Effect of metformin on metabolic improvement and gut
617 microbiota. *Appl. Enviro. Micorb.* 2014; 80:5935-5943. doi:
618 10.1128/AEM.01357-14
619 11. Zhang X, Zhao Y, Xu J, Xue ZS, Zhang MH, Pang XY, Zhang XJ, Zhao LP.
620 Modulation of gut microbiota by berberine and metformin during the treatment of
621 high-fat diet-induced obesity in rats. *Sci Rep.* 2015; 5:14405. doi:
622 10.1038/srep14405
623 12. Zhou ZY, Ren LW, Zhan P, Yang HY, Chai DD, Yu ZW. Metformin exerts
624 glucose-lowering action in high-fat fed mice via attenuating endotoxemia and
625 enhancing insulin signaling. *Acta Pharmacologica Sinica.* 2016; 37: 1063-75. doi:
626 10.1038/aps.2016.21
627 13. Kristoffer F, Falk H, Trine N, Gwen F, Emmanuelle LC, Shinichi S, Edi P,
628 Sara VS, Valborg G, Helle KP, Manimozhiyan A, Karsten K, Anita YV, Henrik
629 V, Rajna H, Paul IC, Jens RK, Junhua L, Torben J, Florence L, Joël D, Søren B,
630 Jeroen R, Torben H, Jun W, Dusko ES, Peer B, and Oluf P. Disentangling the
631 effects of type 2 diabetes and metformin on the human gut microbiota. *Nature.*
632 2015; 528(7581): 262–266. doi: 10.1038/nature15766
633 14. Pedersen HK, Gudmundsdottir V, Nielsen HB, Hyotylainen T, Nielsen T,
634 Jensen BA, Forslund K, Hildebrand F, Prifti E, Falony G, Le Chatelier E,
635 Levenez F, Doré J, Mattila I, Plichta DR, Pöhö P, Hellgren LI, Arumugam M,
636 Sunagawa S, Vieira-Silva S, Jørgensen T, Holm JB, Trošt K; MetaHIT
637 Consortium, Kristiansen K, Brix S, Raes J, Wang J, Hansen T, Bork P, Brunak S,
638 Oresic M, Ehrlich SD, Pedersen O. Human gut microbes impact host serum
639 metabolome and insulin sensitivity. *Nature.* 2016; 535(7612):376-381. doi:

640 10.1038/nature18646
641 15. Jia W, Xie G, Jia W. Bile acid-microbiota crosstalk in gastrointestinal
642 inflammation and carcinogenesis. *Nat. Rev. Gastroenterol Hepatol.*
643 2018;15(2):111-128. doi: 10.1038/nrgastro.2017.119
644 16. Schroeder BO and Backhed F. Signals from the gut microbiota to distant
645 organs in physiology and disease. *Nat. Med.* 2016; 22: 1079-1089. doi:
646 10.1038/nm.4185
647 17. Guo JL, Han X, Tan HY, Huang WD, You YL, Zhan JC. Blueberry extract
648 improves obesity through regulation of the gut microbiota and bile acids via
649 pathways involving FXR and TGR5. iScience. 2019; 19:676-690. doi: 10.1016 /
650 j.isci.2019.08.020
651 18. Sun LL , Xie C, Wang G, Wu Y, Wu Q, Wang XM, Liu J, Deng YY, Xia JL,
652 Bo C, Zhang SY, Chuyu Y, Lian G, Zhang XJ, Zhang H, Bisson WH, Shi JM,
653 Gao XX, Ge PP, Liu CH, Krausz WK, Nicholis RG, Cai JW, Rimal BP, Patterson
654 A, Wang X, Gonzalez FJ, Jiang CT. Gut microbiota and intestinal FXR mediate
655 the clinical benefits of metformin. *Nat Med.* 2018; 24(12): 1919-1929. doi:
656 10.1038/s41591-018-0222-4
657 19. Lee H, Lee Y, Kim J, An J, Lee S, Kong H, Song Y, Lee CK, Kim K.
658 Modulation of the gut microbiota by metformin improves metabolic profiles in
659 aged obese mice. *Gut Microbes.* 2018; 9(2): 155-165. doi:
660 10.1080/19490976.2017.1405209
661 20. Martínez-Moya P, Romero-Calvo I, Requena P, Hernández-Chirlaque C,
662 Aranda CJ, González R, Zarzuelo A, Suárez MD, Martínez-Augustin O, Marín JJ,
663 de Medina FS. Dose-dependent antiinflammatory effect of ursodeoxycholic acid
664 in experimental colitis. *Int Immunopharmacol.* 2013; 15(2): 372–380. doi:
665 10.1016/j.intimp.2012.11.017.
666 21. Renga B, Mencarelli A, Cipriani S, D'Amore C, Carino A, Bruno A,
667 Francisci D, Zampella A, Distrutti E, Fiorucci S. The bile acid sensor FXR is

668 required for immune-regulatory activities of TLR-9 in intestinal inflammation.
669 *PLoS One.* 2013; 8(1): e54472. doi: 10.1371/journal.pone.0054472
670 22. Berger E, Haller D. Structure-function analysis of the tertiary bile acid
671 TUDCA for the resolution of endoplasmic reticulum stress in intestinal epithelial
672 cells. *Biochem Biophys Res Commun.* 2011; 409: 610–615. doi:
673 10.1016/j.bbrc.2011.05.043
674 23. Stenman LK, Holma R, Gylling H, Korpela R. Genetically obese mice do not
675 show increased gut permeability or faecal bile acid hydrophobicity. *Br J Nutr.*
676 2013; 110: 1157–64. doi: 10.1017/S000711451300024X
677 24. Arab JP, Karpen SJ, Dawson PA, Arrese M, Trauner M. Bile acids and
678 nonalcoholic fatty liver disease: Molecular insights and therapeutic perspectives.
679 *Hepatology.* 2017; 65: 350–362. doi: 10.1002/hep.28709
680 25. Wang WJ , Zhao JF, Gui WF, Sun D, Dai HJ, Xiao L, Chu HK, Fan D, Zhu
681 QJ, Bernd S, Huang K, Yang L, and Hou XH. Tauroursodeoxycholic acid inhibits
682 intestinal inflammation and barrier disruption in mice with non-alcoholic fatty
683 liver disease. *British J of Pharmaco.* 2018; 175: 469–484. doi:
684 10.1111/bph.14095
685 26. Xie Q, Khaoustov VI, Chung CC, Sohn J, Krishnan B, Lewis DE, Yoffe B.
686 Effect of tauroursodeoxycholic acid on endoplasmic reticulum stress-induced
687 caspase-12 activation. *Hepatology.* 2002; 36(3): 592–601. doi:
688 10.1053/jhep.2002.35441
689 27. Fondevila C, Shen XD, Tsuchiyashi S, Yamashita K, Csizmadia E, Lassman
690 C, Busuttil RW, Kupiec-Weglinski JM, Bach FH. Biliverdin therapy protects rat
691 livers from ischemia and reperfusion injury. *Hepatology.* 2004; 40: 1333–1341.
692 doi: 10.1002/hep.20480
693 28. Nakao A, Otterbein LE, Overhaus M, Sarady JK, Tsung A, Kimizuka K,
694 Nalesnik MA, Kaizu T, Uchiyama T, Liu F, Murase N, Bauer AJ, Bach FH,
695 Biliverdin protects the functional integrity of a transplanted syngeneic small

696 bowel. *Gastroenterology.* 2004; 127: 595–606. doi: 10.1053/j.gastro.2004.05.059
697 29. Ester GS, Maria JP, Nikolaj SN, Oscar B, Maria JM, Elisa L, Maria AS, Jose
698 JGM. Protective role of biliverdin against bile acid-induced oxidative stress in
699 liver cells. *Free Radical Biology and Medicine.* 2016; 97: 466–477. doi:
700 10.1016/j.freeradbiomed.2016.06.016
701 30. Zhang M, Feng R, Yang M, Qian C, Wang Z, Liu W, Ma J. Effects of
702 metformin, acarbose, and sitagliptin monotherapy on gut microbiota in Zucker
703 diabetic fatty rats. *BMJ Open Diabetes Res Care.* 2019; 7(1):e000717. doi:
704 10.1136/bmjdrc-2019-000717
705 31. Nova E, Pérez de Heredia F, Gómez-Martínez S, Marcos A. The Role of
706 Probiotics on the Microbiota: Effect on Obesity. *Nutr Clin Pract.* 2016;
707 31(3):387-400. doi: 10.1177/0884533615620350
708 32. Zhang WP , Chen LH , Feng H, Wang W, Cai Y, Qi F, Tao XF, Liu J, Shen
709 YJ, Ren XF, Chen X, Xu JM, Shen YX. Rifampicin-induced injury in HepG2
710 cells is alleviated by TUDCA via increasing bile acid transporters expression and
711 enhancing the Nrf2- mediated adaptive response. *Free Radical Biology and*
712 *Medicine.* 2017; 112: 24–35. doi: 10.1016/j.freeradbiomed.2017.07.003
713 33. Navarrete J, Vásquez B, Del SM. Morphoquantitative analysis of the Ileum
714 of C57BL/6 mice (Mus musculus) fed with a high-fat diet. *Int J Clin Exp Pathol.*
715 2015; 8(11):14649-14657.
716 34. Zou CH, Wang YJ, Zhen ZF. 2-NBDG as a fluorescent indicator for direct
717 glucose uptake measurement. *J. Biochem. Biophys. Methods.* 2005; 64: 207–215.
718 doi: 10.1016/j.jbbm.2005.08.001
719 35. Lien F, Berthier A, Bouchaert E, Gheeraert C, Alexandre J, Porez G, Prawitt
720 J, Dehondt H, Ploton M, Colin S, Lucas A, Patrice A, Pattou F, Diemer H, Van
721 Dorsselaer A, Rachez C, Kamilic J, Groen AK, Staels B, Lefebvre P. Metformin
722 interferes with bile acid homeostasis through AMPK-FXR crosstalk. *J. Clin.*
723 *Invest.* 2014; 124(3): 1037–1051. doi: 10.1172/JCI68815.

724 36. Bailey CJ, Wilcock C and Scarpello JH. Metformin and the intestine.
725 *Diabetologia.* 2008; 51: 1552–1553. doi: 10.1007/s00125-008-1053-5
726 37. Canfora EE, Meex R, Venema K, and Blaak EE. Gut microbial metabolites
727 in obesity, NAFLD and T2DM. *Nat. Rev. Endocrinol.* 2019; 15: 261–273. doi:
728 10.1038/s41574-019-0156-z
729 38. Wu H, Esteve E, Tremaroli V, Khan MT, Caesar R, Holm LM, Sthlman M,
730 Olsson L, Serino M, Planas-Fèlix M, Xifra G, Mercader JM, Torrents D, Burcelin
731 R, Ricart W, Perkins R, Fernàndez-Real JM, Bäckhed F. Metformin alters the gut
732 microbiome of individuals with treatment-naive type 2 diabetes, contributing to
733 the therapeutic effects of the drug. *Nat Med.* 2017; 23 (7) :850-868. doi:
734 10.1038/nm.4345
735 39. Nova E, Pérez de Heredia F, Gómez-Martínez S, Marcos A. The Role of
736 Probiotics on the Microbiota: Effect on Obesity. *Nutr Clin Pract.* 2016; 31(3):
737 387-400. doi: 10.1177/0884533615620350
738 40. Sircana A, Framarin L, Leone N, Berrutti M, Castellino F, Parente R,
739 Michieli FD, Paschetta E, Musso G. Altered gut microbiota in type 2 diabetes:
740 just a coincidence? *Curr. Diab. Rep.* 2018; 18(10): 98. doi:
741 10.1007/s11892-018-1057-6
742 41. Kaakoush NO. Insights into the Role of Erysipelotrichaceae in the Human
743 Host. *Front Cell Infect Microbiol.* 2015; 20; 5: 84. doi:
744 10.3389/fcimb.2015.00084
745 42. Turnbaugh PJ, Backhed F, Fulton L, and Gordon JI. Marked alterations in
746 the distal gut microbiome linked to diet-induced obesity. *Cell Host Microbe.*
747 2008; 3(4): 213–223. doi: 10.1016/j.chom.2008.02.015
748 43. Craven M, Egan CE, Dowd SE, McDonough SP, Dogan B, Denkers EY.
749 Inflammation drives dysbiosis and bacterial invasion in murine models of ileal
750 Crohn's disease. *PLoS ONE.* 2012; 7:e41594. doi: 10.1371/journal.pone.0041594
751 44. Nguyen TL, Vieira-Silva S, Liston A, and Raes J. How informative is the

752 mouse for human gut microbiota research? *Dis. Model Mech.* 2015; 8: 1–16. doi:
753 10.1242/dmm.017400.
754 45. Tsung-Ru Wu, Chuan-Sheng Lin, Chih-Jung Chang Tzu-Lung Lin, Jan
755 Martel, Yun-Fei Ko, David M Ojcius, Chia-Chen Lu, John D Young,1 Hsin-Chih
756 Lai. Gut commensal *Parabacteroides goldsteinii* plays a predominant role in the
757 anti-obesity effects of polysaccharides isolated from *Hirsutella sinensis*. *Gut*
758 2018;0:1–14. doi: 10.1136/gutjnl-2017-315458
759 46. Manley S, Ding WX. Role of farnesoid X receptor and bile acids in alcoholic
760 liver disease. *Acta Pharmaceutica Sinica B.* 2015;5(2):158–167. doi:
761 10.1016/j.apsb.2014.12.011
762 47. Anhê FF, Roy D, Pilon G, Dudonne S, Matamoros S, Varin T, Marette A. A
763 polyphenol-rich cranberry extract protects from diet-induced obesity, insulin
764 resistance and intestinal inflammation in association with increased *akkermansia*
765 *spp*. population in the gut microbiota of mice. *Gut.* 2015; 64(6): 872–883.
766 doi:10.1136/gutjnl-2014-307142
767 48. Rodriguez J, Hiel S, Delzenne NM. Metformin: old friend, new ways of
768 action-implication of the gut microbiome? *Curr Opin Clin Nutr Metab Care.*
769 2018; 21(4): 294-301. doi: 10.1097/MCO.0000000000000468
770 49. Everard A, Belzer C, Geurts L, Ouwerkerk JP, Druart C, Bindels LB, Guiot
771 Y, Derrien M, Muccioli GG, Delzenne NM, de Vos WM, Cani PD. Cross-talk
772 between *Akkermansia muciniphila* and intestinal epithelium controls diet-induced
773 obesity. *Proc Natl Acad Sci USA.* 2013; 110(22):9066-9071. doi:
774 10.1073/pnas.1219451110
775 50. Dempsey JL, Wang D, Siginir G, Fei Q, Raftery D, Gu H, Yue Cui J.
776 Pharmacological Activation of PXR and CAR Downregulates Distinct Bile
777 Acid-Metabolizing Intestinal Bacteria and Alters Bile Acid Homeostasis. *Toxicol*
778 *Sci.* 2019;168(1):40-60. doi: 10.1093/toxsci/kfy271
779 51. Wahlstrom A, Sayin SI, Marschall HU, Backhed F. Intestinal crosstalk

780 between bile acids and microbiota and its impact on host metabolism. *Cell Metab.*
781 2016; 24, 41–50. doi: 10.1016/j.cmet.2016.05.005
782 52. Li F, Jiang CT, Krausz KW, Li YF, Albert I, Hao HP, Fabre KM, Mitchell
783 JB, Patterson A, Gonzalez FJ. Microbiome remodelling leads to inhibition of
784 intestinal farnesoid X receptor signalling and decreased obesity. *Nat. Commun.*
785 2013; 4: 2384. doi: 10.1038/ncomms3384
786 53. Choi YJ, Shin HS, Choi HS, Park JW, Jo I, Oh ES, Lee KY, Lee BH,
787 Johnson R, Kang DH. Uric acid induces fat accumulation via generation of
788 endoplasmic reticulum stress and SREBP-1c activation in hepatocytes. *Lab Invest.*
789 2014; 94(10): 1114–1125. doi: 10.1038/labinvest.2014.98
790 54. Legry V, Van Rooyen DM, Lambert B, Sempoux C, Poekes L,
791 Español-Suñer R, Molendi-Coste O, Horsmans Y, Farrell GC, Leclercq IA.
792 Endoplasmic reticulum stress does not contribute to steatohepatitis in obese and
793 insulin-resistant high-fat-diet-fed foz/foz mice. *Clin Sci (Lond).* 2014;
794 127(7):507-518. doi: 10.1042/CS20140026
795 55. Cao YN, Xue Y, Xue L, Jiang XL, Wang XL, Zhang ZJ, Yang J, Lu JL,
796 Zhang CX, Wang WQ, Ning G. Hepatic menin recruits SIRT1 to control liver
797 steatosis through histone deacetylation. *J Hepatol.* 2013; 59(6): 1299-1306. doi:
798 10.1016/j.jhep.2013.07.011
799 56. Fazakerley DJ, Chaudhuri R, Yang PY, Maghzal GJ, Thomas KC, Krycer
800 JR, Humphrey SJ, Parker BL, Fisher-Wellman KH, Meoli CC, Hoffman NJ,
801 Diskin C, Burchfield JG, Cowley MJ, Kaplan W, Modrusan Z, Kolumam G,
802 Yang KYL, Chen DL, Samocha-Bonet D, Greenfield JR, Hoehn JL, Stocker R,
803 James DE. Mitochondrial CoQ deficiency is a common driver of mitochondrial
804 oxidants and insulin resistance. *eLife* . 2018; 7:e32111. doi: 10.7554/eLife.32111
805 57. Hancock M, Hafstad AD, Nabeebaccus AA, Catibog N, Logan A, Smyrnias
806 L, Hansen SS, Lanner J, Schröder K, Murphy MP, Shah MA, Zhang M.
807 Myocardial NADPH oxidase-4 regulates the physiological response to acute

808 exercise. *eLife*. 2018;7:e41044. doi: 10.7554/eLife.41044
809 58. Hu H, Fan X, Guo Q, Wei X, Yang D, Zhang B, Liu J, Wu Q, Oh Y, Feng Y,
810 Chen K, Hou L, Gu N. Silicon dioxide nanoparticles induce insulin resistance
811 through endoplasmic reticulum stress and generation of reactive oxygen species.
812 *Part Fibre Toxicol.* 2019;16(1):41. doi: 10.1186/s12989-019-0327-z
813 59. You L, Yang C, Du Y, Liu Y, Chen G, Sai N, Dong X, Yin X, Ni J. Matrine
814 Exerts Hepatotoxic Effects via the ROS-Dependent Mitochondrial Apoptosis
815 Pathway and Inhibition of Nrf2-Mediated Antioxidant Response. *Oxid Med Cell*
816 *Longev.* 2019; 2019:1045345. doi: 10.1155/2019/1045345
817 60. Takafumi S, Shiori S, Keiichiro H, Eriko N, Eri HK, Ayaka Y, Liam B,
818 Nobuyuki T, Hiroshi S, Masayuki Y. Hyperactivation of Nrf2 in early tubular
819 development induces nephrogenic diabetes insipidus. *Nat Commun.* 2017;
820 8:14577. doi: 10.1038/ncomms14577
821 61. Manuel M, Katrin F, and Elke HH. Activation of Nrf2 signaling by natural
822 products-can it alleviate diabetes? *Biotechnol Adv.* 2018; 36(6): 1738–1767. doi:
823 10.1016/j.biotechadv.2017.12.015
824 62. Annika SA, Emily T, Brig M, Shaji C, Hannah AN, Yunzhao T, Jed WF,
825 Jonathan MJD, Claes BW, Nils W, Morey WH, Stephen HF, Hindrik M, Anders
826 HR. Sulforaphane reduces hepatic glucose production and improves glucose
827 control in patients with type 2 diabetes. *Sci Transl Med.* 2017; 9(394). pii:
828 eaah4477. doi: 10.1126/scitranslmed.aah4477
829

830 **Figure captions**

831 **Figure 1. Metformin prevents obesity and systemic metabolic disorders in obese**
832 **mice induced by HFD.** Boy weight (A), weight gain (B), food intake (C), H&E
833 staining of epididymal adipose tissue (D, 400×), number of adipocytes (E), levels of
834 total cholesterol and triacylglycerol in liver (F) and serum (G), and serum FFA (H)
835 are shown. Data are expressed as the mean ± SD. *$P < 0.05$, **$P < 0.01$ and ***$P <$
836 0.001.

837 **Figure 2. Metformin improves glucose homeostasis and insulin sensitivity in**
838 **diet-induced obese mice.** IPGTT (A); AUC of IPGTT (B); IPITT (C); slope of IPITT
839 (D) measured at the end of the experimental period. Serum level of FBG (E), FINS
840 (F), and HOMA-IR (G). Protein expression of Akt, phosphorylated Akt, IRS-1,
841 phosphorylated IRS-1 Ser307 and quantitative analysis for the densitometry of
842 pIRS-1 and p-Akt protein level(H). Data are expressed as mean ± SD. *$P < 0.05$, **P
843 < 0.01 and ***$P < 0.001$.

844 **Figure 3. Metformin blunts intestinal and liver inflammation.** Determination of
845 inflammatory factors in liver (A) and ileum (B) by qPCR and serum LPS (C) by kit.
846 Expression levels of IκB, phosphorylated IκB, P65, and phosphorylated P65 as
847 determined by western blot and quantitative analysis for the densitometry of p-IκB
848 and p-P65 protein level (D). Data are expressed as mean ± SD. *$P < 0.05$, **$P < 0.01$
849 and ***$P < 0.001$.

850 **Figure 4. Metformin ameliorates HFD-induced oxidative stress.** Representative
851 markers of oxidative stress level: CAT (A), MDA (B), and GSH:GSSG ratio in the
852 liver (C). Protein expression of total Nrf2, phosphorylated Nrf2, total AMPK, and
853 phosphorylated AMPK; quantitative analysis for the densitometry of the p-Nrf2 and
854 p-AMPK protein (D). Quantitative RT-PCR analysis of *Nrf2, Keap1* and
855 representative downstream genes (*Nqo1* and *Ho-1*) (E). Data are expressed as mean ±
856 SD. *$P < 0.05$, **$P < 0.01$ and ***$P < 0.001$.

857 **Figure 5. Metformin remodels fecal microbial structure and communities.**
858 Microbial composition with cluster at the phylum level (A); relative abundance of gut
859 microbiota at the phylum level (B); ratio of Bacteroidetes to Firmicutes (C); function
860 analysis of gut microbiota (D). Data are represented as mean ± SD. *$P < 0.05$ and **P
861 < 0.01.

862 **Figure 6. Genus-based comparison of microbial similarities and differences.**
863 Heatmap showing clustering of bacterial communities with their relative abundances
864 at the genus level (A). The bacterial communities or OTUs were clustered
865 phylogenetically by neighbor-joining method and the libraries were clustered by
866 profile pattern using Unifrac analysis. Relative abundances (log values) of microbial
867 genus are displayed in a red-to-blue color code (high to low abundance). Linear
868 discriminant analysis (LDA) score for taxa differing between treatment groups (B).
869 LDA scores with threshold > 3 indicated a higher relative abundance in the
870 corresponding group than in the other two groups.

871 **Figure 7. Differential metabolites determined by non-targeted metabolomics.**
872 Metabolite clustering heat map (A); OPLS-DA score plot (B), in the OPLS-DA score
873 plot, each data point represents one sample, and the distance between points in the
874 plot indicates the similarity between samples; number of different metabolites
875 between each group (C), the major upregulated differential metabolites (D).

876 **Figure 8. Correlation heatmap for gut microorganisms and metabolites.** Matrix
877 heatmap showing the correlation between gut microbiota and metabolome at Phylum
878 (A) and Species (B) levels. Growth curve of *A. muciniphila* in the presence of
879 metformin or TUDCA (C).

880 **Figure 9. TUDCA alleviates insulin resistance caused by PA.** Glucose uptake (A)
881 and the blood glucose remaining in supernatant (B). Protein levels of p-Akt, Akt,
882 pIRS-1 Ser307, IRS-1 were determined by western blot (C). Data are expressed as the
883 mean ± SD. *$P < 0.05$, **$P < 0.01$ and ***$P < 0.001$.

884 **Figure 10. TUDCA relieves PA-induced insulin resistance via activating**
885 **Nrf2/ARE signaling pathway.** Intracellular ROS content (A); the ratio of
886 GSH/GSSG (B); Protein levels of p-Nrf2 and Nrf2 were determined by western blot
887 (C); Quantitative RT-PCR analysis of *Nrf2*, representative Nrf2 downstream genes
888 *Ho-1* and *Nqo1* (D); Under Nrf2 knock-down, glucose uptake (E) and blood glucose
889 in the medium supernatant (F) are shown. Data are expressed as mean ± SD. *P <
890 0.05, **P < 0.01 and ***P < 0.001.

891 **Figure 11. Metformin increases hepatic TUDCA.** The content of TUDCA in the
892 liver was determined using HPLC (A), and the relative mRNA levels of bile acid
893 synthetase (*Cyp7a1*, *Cyp27a1*, *Baat*) determined by qPCR (B).

894

895 **Table 1. Diversity of gut microbiota in HFD and HFD+Met treated mice**

Groups	Reads	OTUs	Observed species	Ace	Chao1	Shannon	Simpson
NCD	78316±4945	372±35	330±21	345±17	350±21	5.10±0.67	0.92±0.04
HFD	76154±7745	350±40	312±20	325±24	326±24	5.38±0.33	0.95±0.02
HFD+Met	80004±421	374±21	335±20*	342±22*	348±20*	5.24±0.27	0.95±0.02

896 Data are expressed as mean ± SD.

897 * Indicates significantly different from the HFD group at the *$P < 0.05$ level.

898

Figure 1

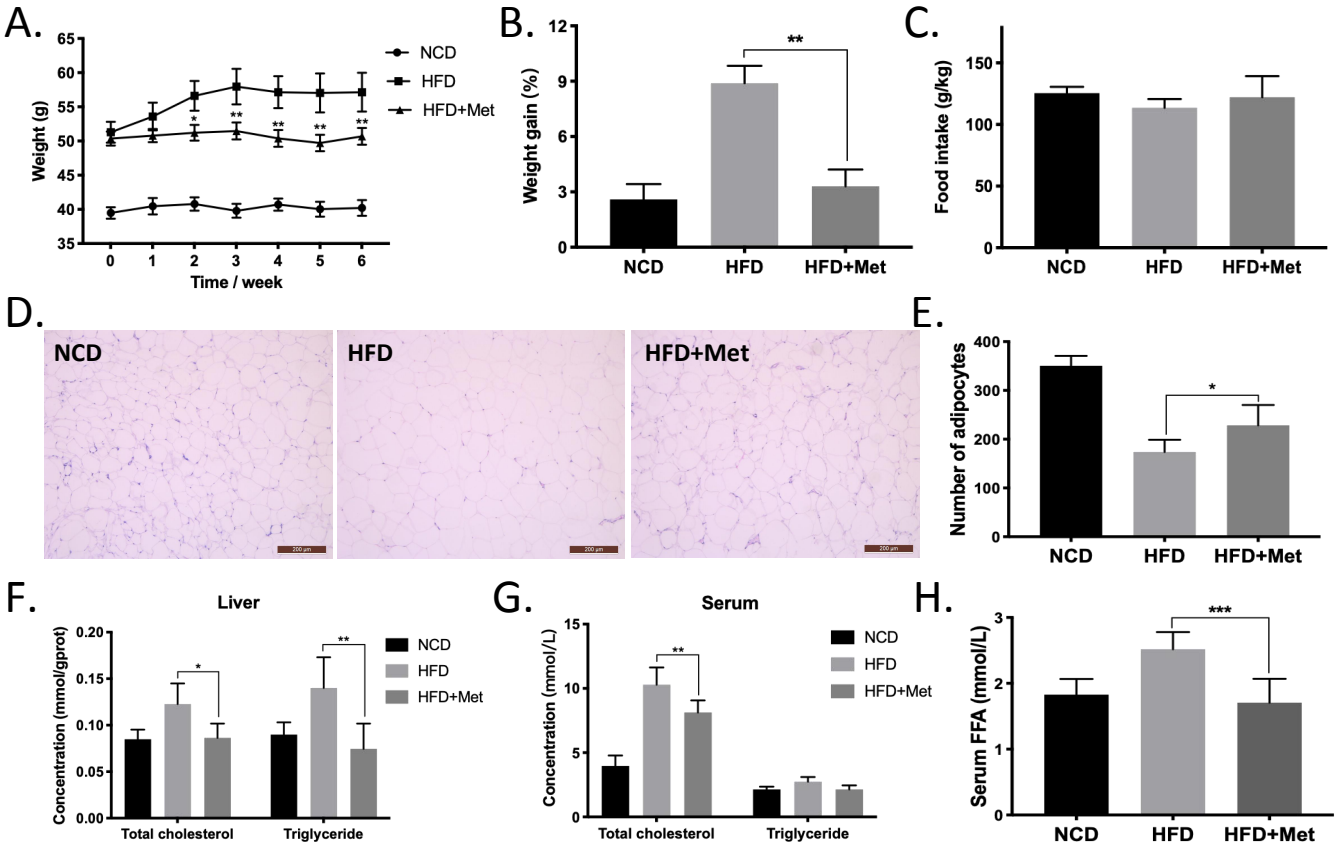
A.
Weight (g)
Time / week
NCD
HFD
HFD+Met
B.
Weight gain (%)
NCD
HFD
HFD+Met
C.
Food intake (g/kg)
NCD
HFD
HFD+Met
D.
NCD
HFD
HFD+Met
E.
Number of adipocytes
NCD
HFD
HFD+Met
F.
Liver
Concentration (mmol/gprot)
Total cholesterol
Triglyceride
NCD
HFD
HFD+Met
G.
Serum
Concentration (mmol/L)
Total cholesterol
Triglyceride
NCD
HFD
HFD+Met
H.
Serum FFA (mmol/L)
NCD
HFD
HFD+Met

Figure 2

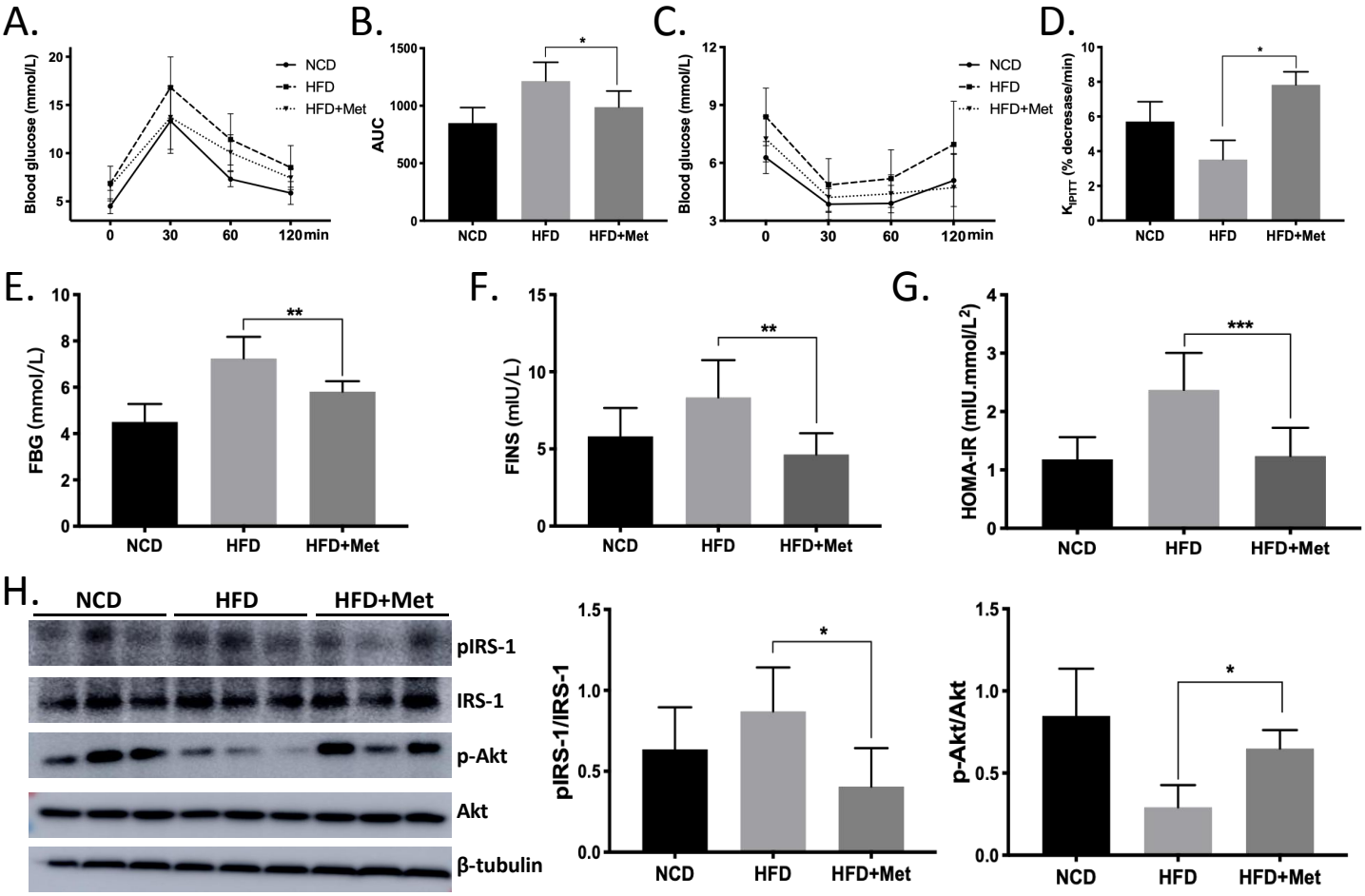
A.
Blood glucose (mmol/L)
NCD
HFD
HFD+Met
0
30
60
120min
B.
AUC
NCD
HFD
HFD+Met
C.
Blood glucose (mmol/L)
D.
K_{IPITT} (% decresase/min)
E.
FBG (mmol/L)
F.
FINS (mIU/L)
G.
HOMA-IR (mIU.mmol/L^2)
H.
pIRS-1
IRS-1
p-Akt
Akt
β-tubulin
pIRS-1/IRS-1
p-Akt/Akt

Figure 3

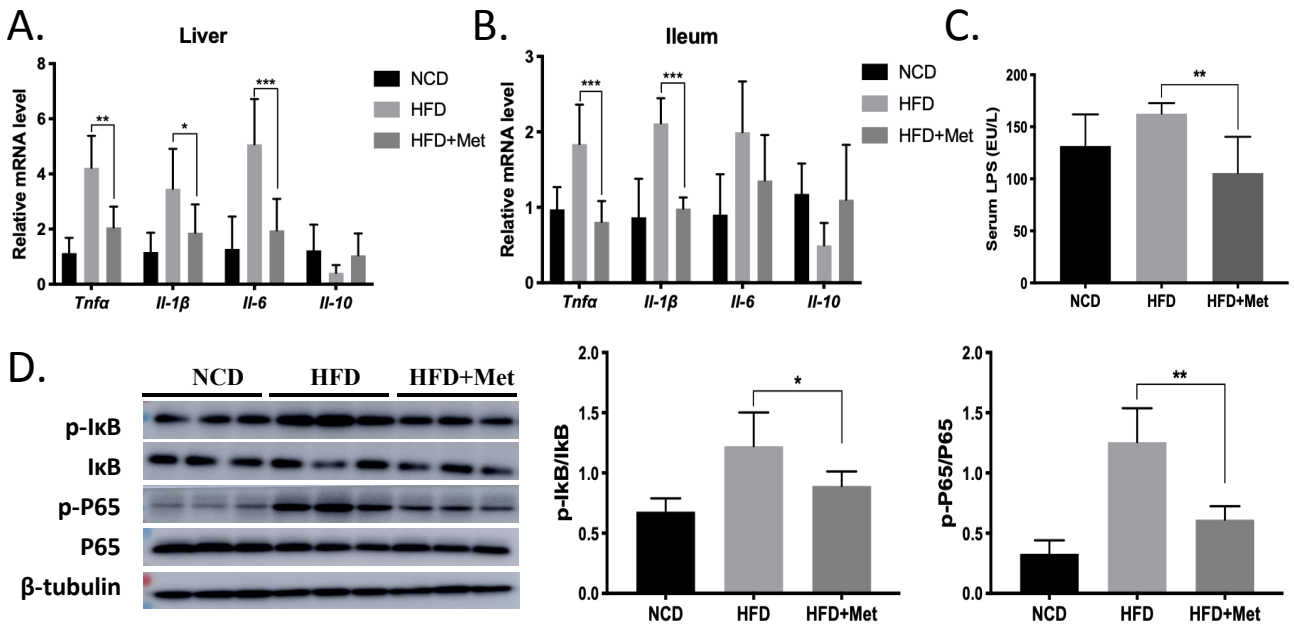
A.
Liver
Relative mRNA level
NCD
HFD
HFD+Met
Tnfα
Il-1β
Il-6
Il-10
B.
Ileum
C.
Serum LPS (EU/L)
D.
NCD
HFD
HFD+Met
p-IκB
IκB
p-P65
P65
β-tubulin
p-IkB/IkB
p-P65/P65

Figure 4

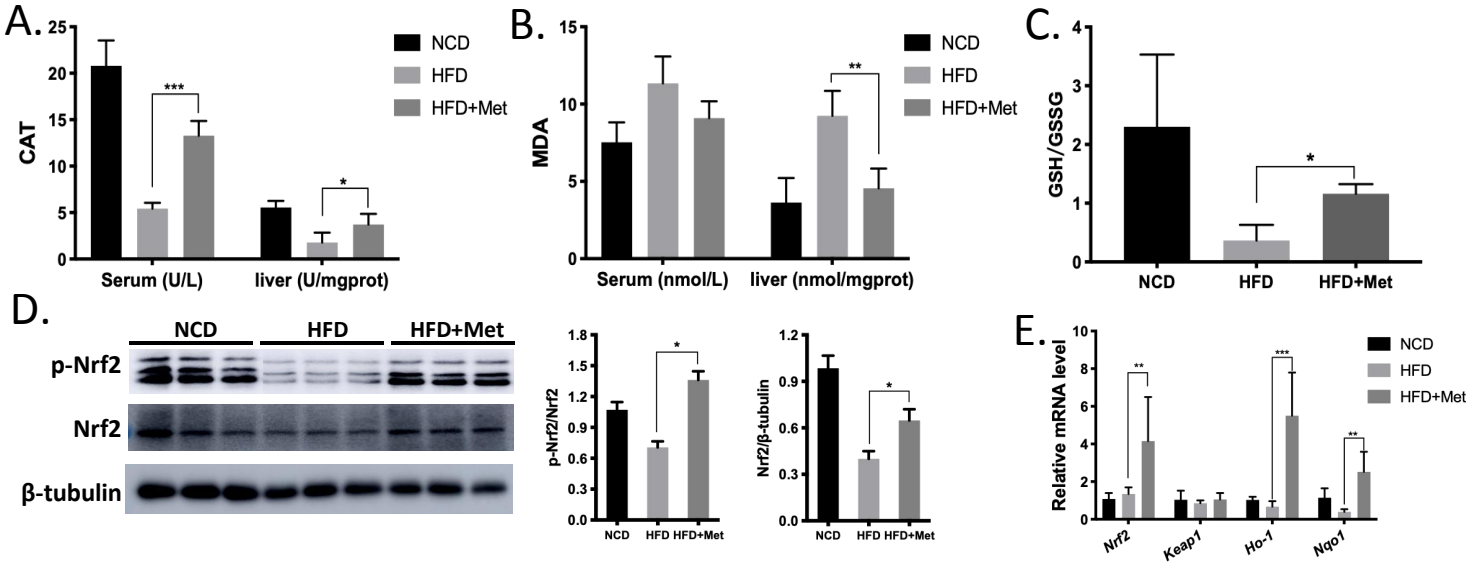
A.
CAT
NCD
HFD
HFD+Met
Serum (U/L)
liver (U/mgprot)
B.
MDA
Serum (nmol/L)
liver (nmol/mgprot)
C.
GSH/GSSG
D.
p-Nrf2
Nrf2
β-tubulin
p-Nrf2/Nrf2
Nrf2/β-tubulin
E.
Relative mRNA level
Nrf2
Keap1
Ho-1
Nqo1

Figure 5

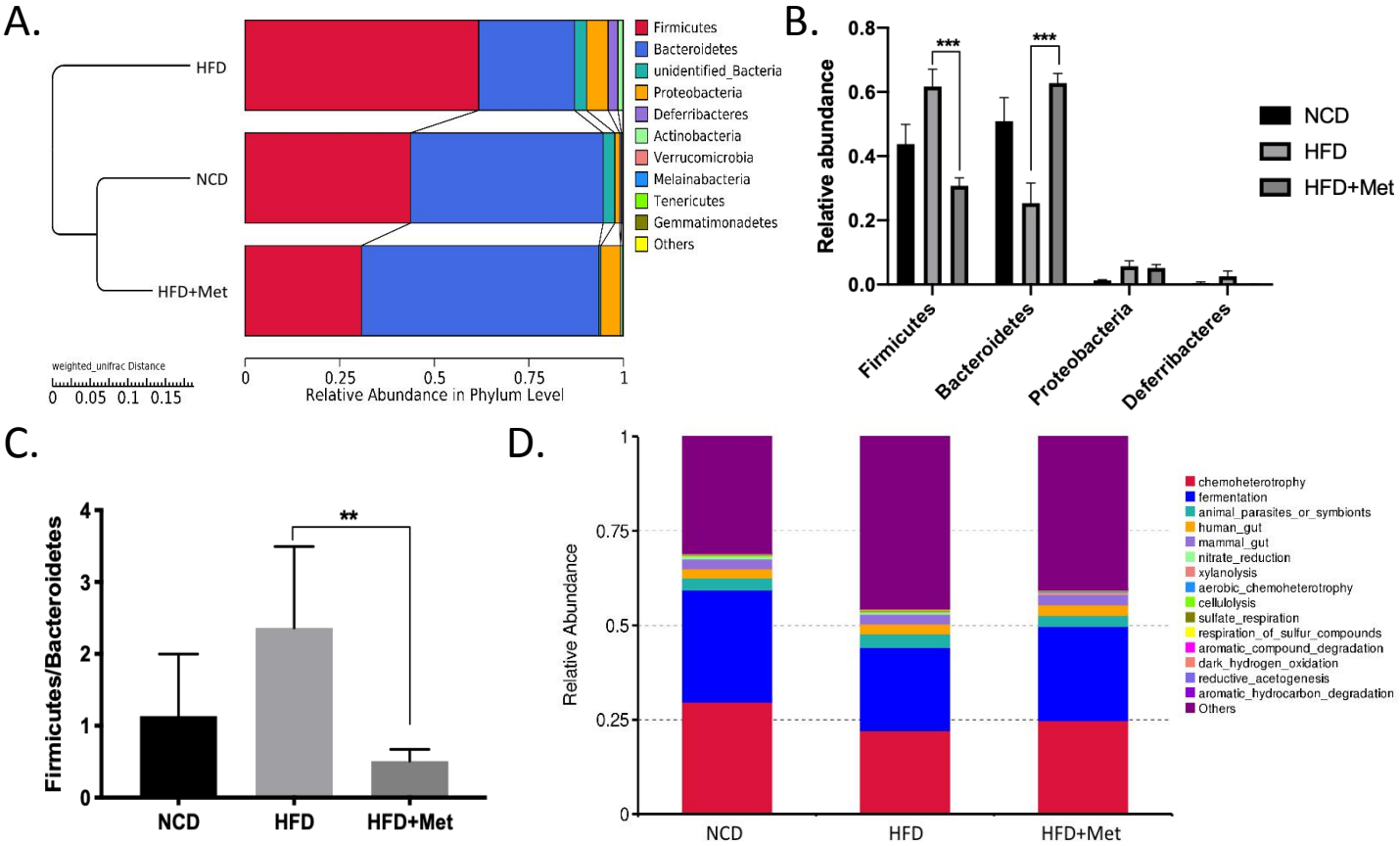
A.
HFD
NCD
HFD+Met
Firmicutes
Bacteroidetes
unidentified_Bacteria
Proteobacteria
Deferribacteres
Actinobacteria
Verrucomicrobia
Melainabacteria
Tenericutes
Gemmatimonadetes
Others
weighted_unifrac Distance
0 0.05 0.1 0.15
0 0.25 0.5 0.75 1
Relative Abundance in Phylum Level
B.
Relative abundance
0.0 0.2 0.4 0.6 0.8
***
***
NCD
HFD
HFD+Met
Firmicutes
Bacteroidetes
Proteobacteria
Deferribacteres
C.
Firmicutes/Bacteroidetes
0 1 2 3 4
**
NCD
HFD
HFD+Met
D.
Relative Abundance
0 0.25 0.5 0.75 1
NCD
HFD
HFD+Met
chemoheterotrophy
fermentation
animal_parasites_or_symbionts
human_gut
mammal_gut
nitrate_reduction
xylanolysis
aerobic_chemoheterotrophy
cellulolysis
sulfate_respiration
respiration_of_sulfur_compounds
aromatic_compound_degradation
dark_hydrogen_oxidation
reductive_acetogenesis
aromatic_hydrocarbon_degradation
Others

Figure 6

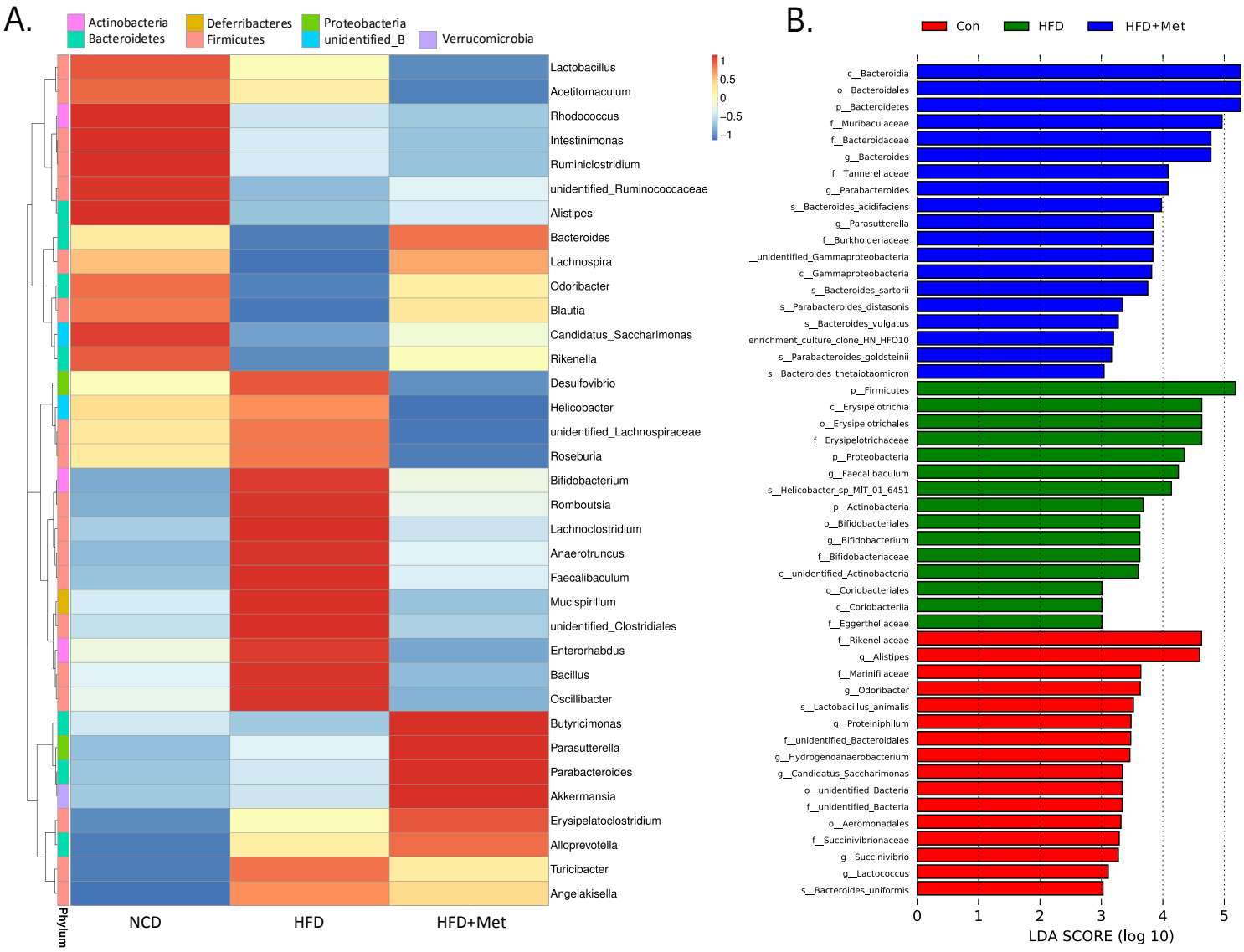
A.
Actinobacteria
Bacteroidetes
Deferribacteres
Firmicutes
Proteobacteria
unidentified_B
Verrucomicrobia
Lactobacillus
Acetitomaculum
Rhodococcus
Intestinimonas
Ruminiclostridium
unidentified_Ruminococcaceae
Alistipes
Bacteroides
Lachnospira
Odoribacter
Blautia
Candidatus_Saccharimonas
Rikenella
Desulfovibrio
Helicobacter
unidentified_Lachnospiraceae
Roseburia
Bifidobacterium
Romboutsia
Lachnoclostridium
Anaerotruncus
Faecalibaculum
Mucispirillum
unidentified_Clostridiales
Enterorhabdus
Bacillus
Oscillibacter
Butyricimonas
Parasutterella
Parabacteroides
Akkermansia
Erysipelatoclostridium
Alloprevotella
Turicibacter
Angelakisella
1
0.5
0
−0.5
−1
Phylum
NCD
HFD
HFD+Met
B.
Con
HFD
HFD+Met
c__Bacteroidia
o__Bacteroidales
p__Bacteroidetes
f__Muribaculaceae
f__Bacteroidaceae
g__Bacteroides
f__Tannerellaceae
g__Parabacteroides
s__Bacteroides_acidifaciens
g__Parasutterella
f__Burkholderiaceae
__unidentified_Gammaproteobacteria
c__Gammaproteobacteria
s__Bacteroides_sartorii
s__Parabacteroides_distasonis
s__Bacteroides_vulgatus
enrichment_culture_clone_HN_HFO10
s__Parabacteroides_goldsteinii
s__Bacteroides_thetaiotaomicron
p__Firmicutes
c__Erysipelotrichia
o__Erysipelotrichales
f__Erysipelotrichaceae
p__Proteobacteria
g__Faecalibaculum
s__Helicobacter_sp_MIT_01_6451
p__Actinobacteria
o__Bifidobacteriales
g__Bifidobacterium
f__Bifidobacteriaceae
c__unidentified_Actinobacteria
o__Coriobacteriales
c__Coriobacteriia
f__Eggerthellaceae
f__Rikenellaceae
g__Alistipes
f__Marinifilaceae
g__Odoribacter
s__Lactobacillus_animalis
g__Proteiniphilum
f__unidentified_Bacteroidales
g__Hydrogenoanaerobacterium
g__Candidatus_Saccharimonas
o__unidentified_Bacteria
f__unidentified_Bacteria
o__Aeromonadales
f__Succinivibrionaceae
g__Succinivibrio
g__Lactococcus
s__Bacteroides_uniformis
0
1
2
3
4
5
LDA SCORE (log 10)

Figure 7

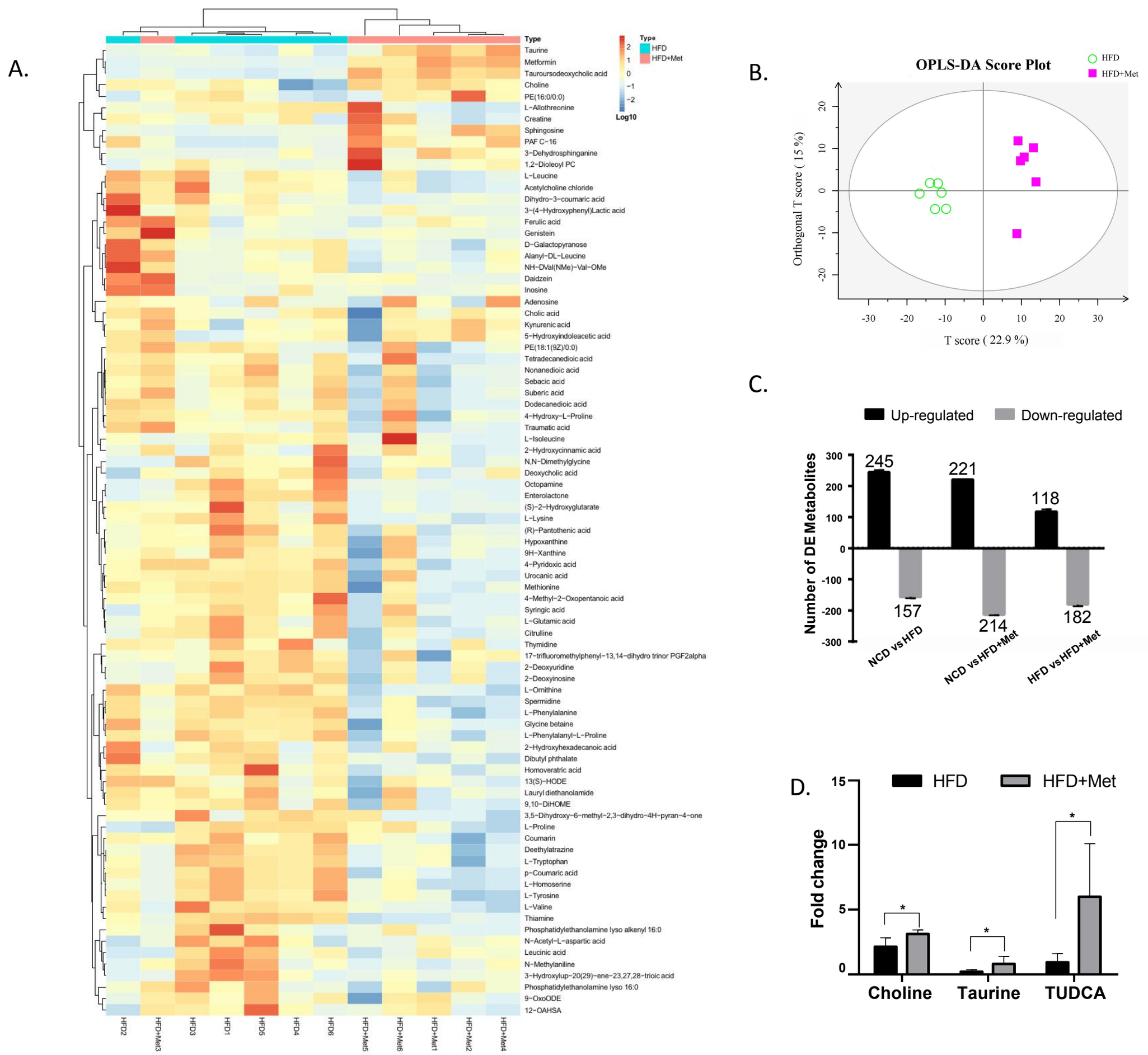
A.
Type
HFD
HFD+Met
Log10
B.
OPLS-DA Score Plot
HFD
HFD+Met
Orthogonal T score (15 %)
T score (22.9 %)
C.
Up-regulated
Down-regulated
Number of DE Metabolites
245
221
118
157
214
182
NCD vs HFD
NCD vs HFD+Met
HFD vs HFD+Met
D.
HFD
HFD+Met
Fold change
Choline
Taurine
TUDCA

Figure 8

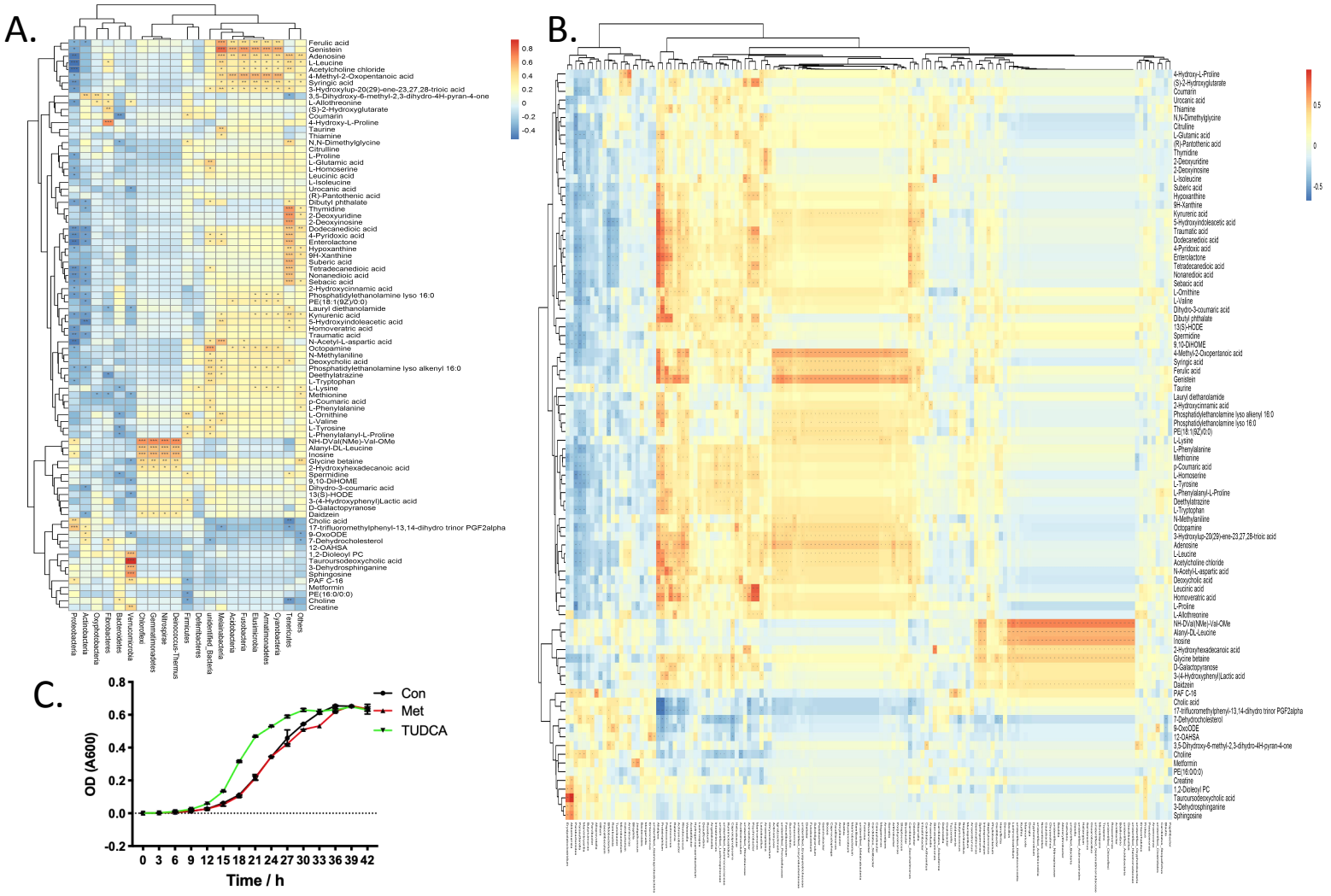

Figure 9

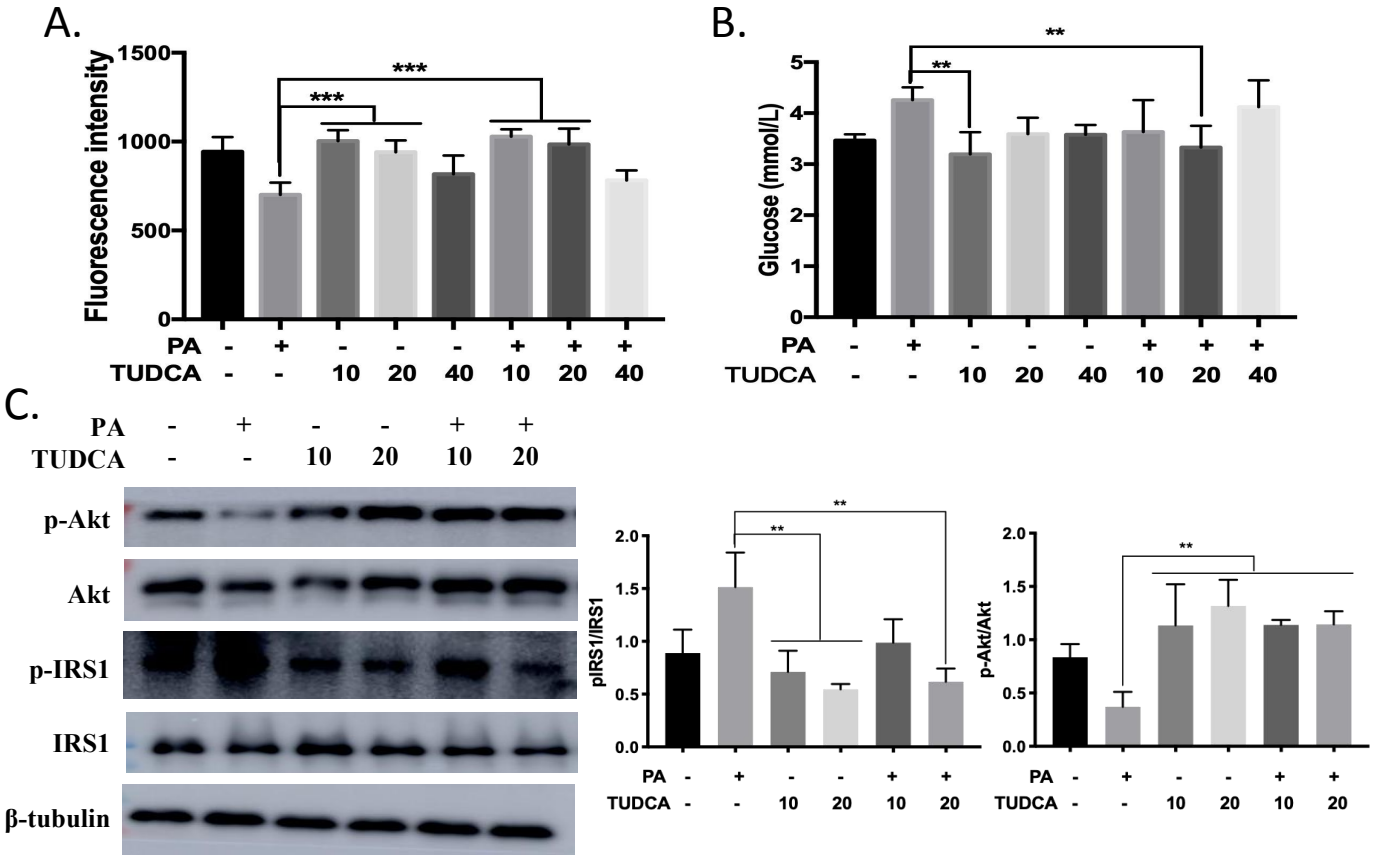
A.
Fluorescence intensity
1500
1000
500
0
***
***
PA - + - - - + + +
TUDCA - - 10 20 40 10 20 40
B.
Glucose (mmol/L)
5
4
3
2
1
0
**
**
PA - + - - - + + +
TUDCA - - 10 20 40 10 20 40
C.
PA - + - - + +
TUDCA - - 10 20 10 20
p-Akt
Akt
p-IRS1
IRS1
β-tubulin
pIRS1/IRS1
2.0
1.5
1.0
0.5
0.0
**
**
PA - + - - + +
TUDCA - - 10 20 10 20
p-Akt/Akt
2.0
1.5
1.0
0.5
0.0
**
PA - + - - + +
TUDCA - - 10 20 10 20

Figure 10

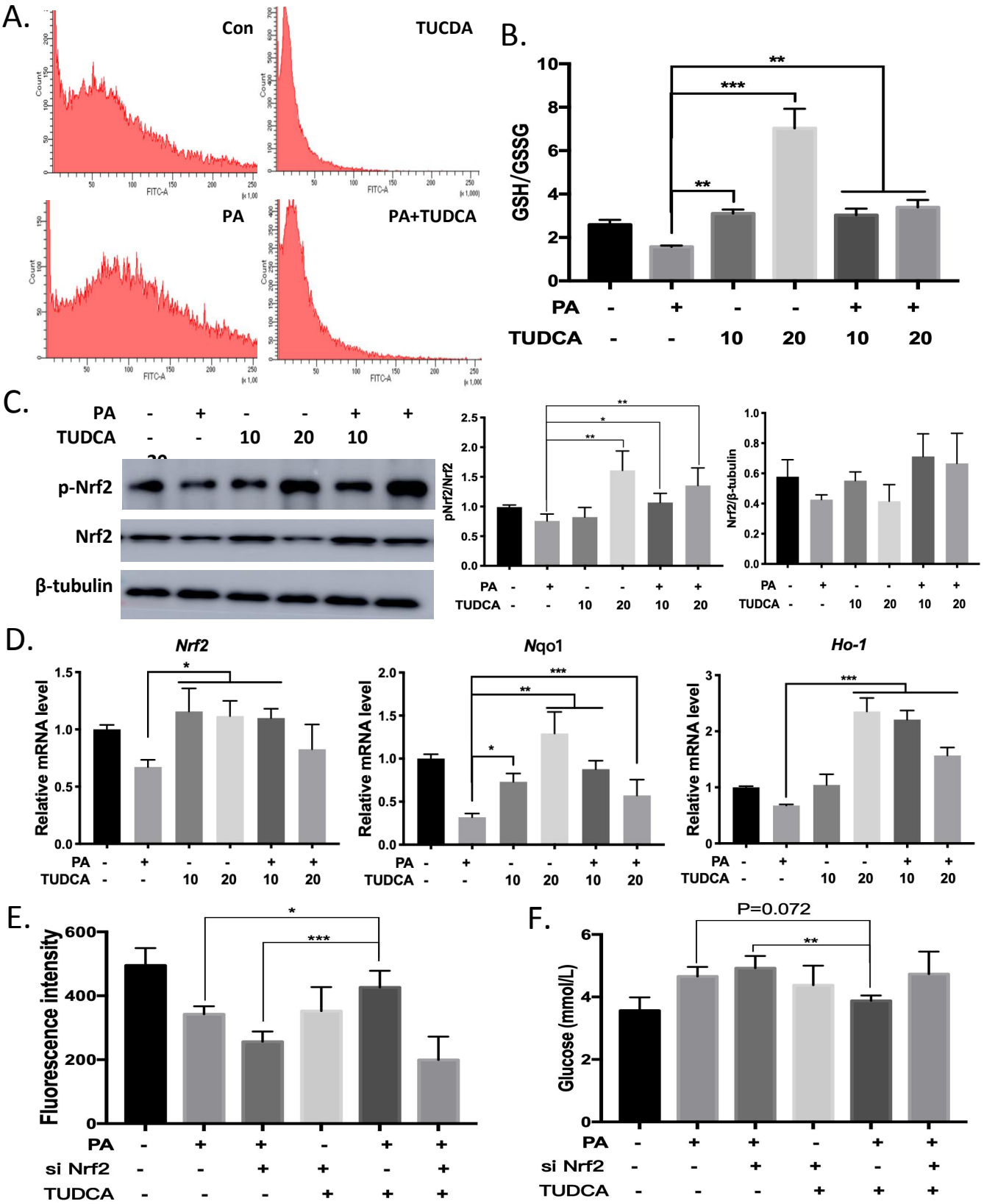
A.
Con
TUCDA
PA
PA+TUDCA
B.
GSH/GSSG
PA
TUDCA
C.
PA
TUDCA
p-Nrf2
Nrf2
β-tubulin
pNrf2/Nrf2
Nrf2/β-tubulin
D.
Nrf2
Nqo1
Ho-1
Relative mRNA level
E.
Fluorescence intensity
PA
si Nrf2
TUDCA
F.
P=0.072
Glucose (mmol/L)

Figure 11

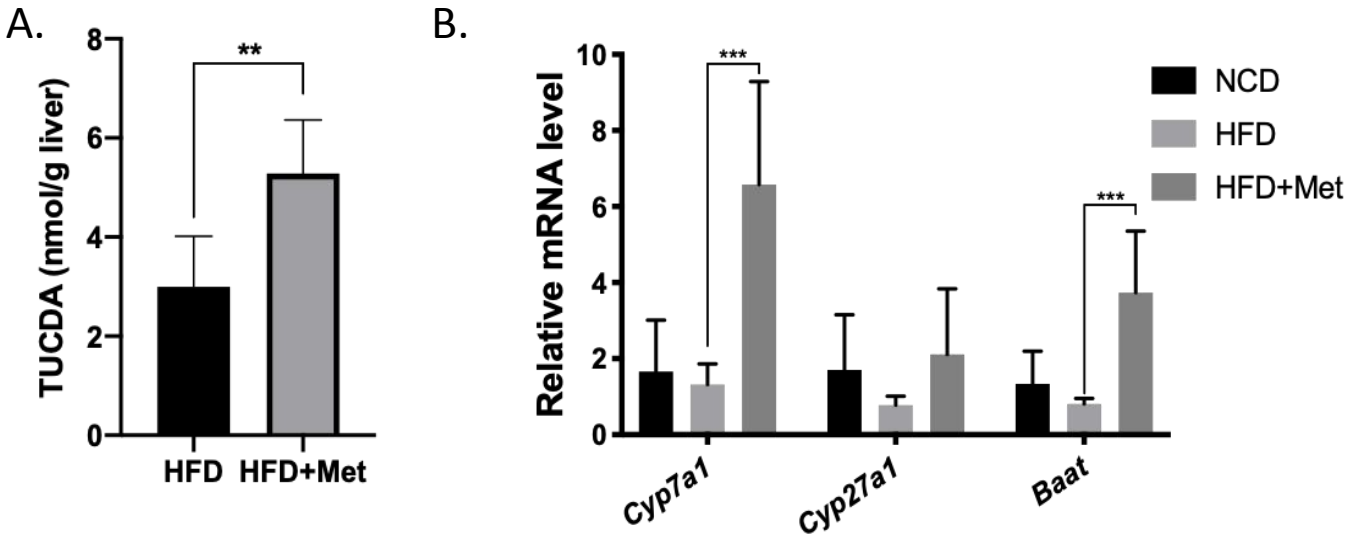
A.
TUCDA (nmol/g liver)
8
6
4
2
0
**
HFD
HFD+Met
B.
Relative mRNA level
10
8
6
4
2
0
***
***
NCD
HFD
HFD+Met
Cyp7a1
Cyp27a1
Baat